South American Cold Surges: Types, Composites, and Case Studies

ANTHONY R. LUPO,* JOSEPH J. NOCERA, LANCE F. BOSART, ERIC G. HOFFMAN, AND DAVID J. KNIGHT

Department of Earth and Atmospheric Sciences, The University at Albany, State University of New York, Albany, New York

(Manuscript received 28 September 1999, in final form 26 September 2000)

ABSTRACT

This paper examines the climatological, large-scale, and synoptic-scale aspects of South American cold surges using NCEP–NCAR gridded reanalyses for the 1992–96 period. Three common cold surge types are identified on the basis of a thickness (1000–850 hPa) criteria: type 1—a transient surge associated with weak anticyclone development east of the Andes in the absence of ridging aloft, type 2—a strong and persistent surge associated with dynamic anticyclogenesis aloft and strong surface anticyclone development east of the Andes, and type 3—a surge east of the Brazilian coastal mountains. Cold surges are most common during the winter and spring (Jun–Nov), accounting for 189 of the 256 events (74%).

Case studies of two events (19–22 Jul 1992 and 12–14 Apr 1993) are conducted from both a conventional isobaric and a potential vorticity (PV) perspective. The upper-air flow pattern in the July 1992 type 2 case is characterized by the presence of a strong ridge–trough couplet, which amplifies and becomes quasi-stationary, allowing for a deep layer of equatorward flow over South America. Dynamically, this flow pattern favors the development of a very strong surface anticyclone to the east of the Andes in response to a combination of differential anticyclonic vorticity advection, low-level cold advection, and, equivalently, positive PV advection. Because of the associated cold air damming east of the Andes, modified cool air is transported into the western part of Amazonia. Cold air damming east of the Brazilian coastal mountains is associated with the transition of the July 1992 type 2 surge into a type 3 surge.

The cold surge of April 1993 is examined as a rare event that does not fit the above classification. It is characterized by explosive cyclogenesis close to the coast of Argentina. Unlike the representative type 2 cold surge of July 1992, which tends to occur in association with southwesterly flow aloft, the April 1993 cold surge occurs beneath westerly and northwesterly flow aloft. Cold air penetration into lower latitudes is restricted because the geostrophic wind has a component directed away from the Andes equatorward of the cyclone. The dynamical forcing mechanisms associated with the April 1993 event are of smaller scale than those of the much more common surges typified by the July 1992 event.

1. Introduction

In the past, there have been relatively few studies that have examined the characteristics of South America cold surges [e.g., Marengo et al. (1997a,b); selected previous South American cold-air surge studies are listed in Table 1] as compared to studies of cold surges in the Northern Hemisphere (e.g., Boyle and Chen 1987; Mecikalski and Tilley 1992; Reding 1992; Konrad 1996; Schultz et al. 1997, 1998). Cold surges in South America can occur frequently during the Southern Hemisphere winter season, and these surges can penetrate deep into subtropical (and even tropical) South America (e.g., Myers 1964; Parmenter 1976; Fortune and Kousky 1983; Garreaud 1999, 2000). They can also occur during the warm season (Garreaud and Wallace 1998). Just as these strong cold surges can threaten the agricultural interests of the southeastern United States (e.g., Quiroz 1984; Rogers and Rohli 1991), South American cold surges can cause economic hardship to the farmers of Brazilian staple crops (e.g., Hamilton and Tarifa 1978; Marengo et al. 1997a,b). Thus, it is imperative to describe the occurrence of, and the atmospheric processes that contribute to, the occurrence of these cold surges in order to improve the forecasting of these events, thereby minimizing the economic impact of these events.

Cold surges in the Northern Hemisphere have been associated with highly amplified upper-level (500–200 hPa) planetary-scale waves, especially upstream ridging and/or upstream or downstream blocking (e.g., Rex

* Current affiliation: Department of Soil and Atmospheric Sciences, University of Missouri—Columbia, Columbia, Missouri.

Corresponding author address: Anthony R. Lupo, Department of Soil and Atmospheric Sciences, 109 Gentry Hall, University of Missouri—Columbia, Columbia, MO 65211.
E-mail: LupoA@missouri.edu

TABLE 1. Selected previous South American cold air surge studies.

Author	Type	Application
Sera and Ratisbona (1945)	Climatology	Anticyclones (surface data only)
Myers (1964)	Synoptic case study (surface observations only)	Cross-equatorial cold front passage into Venezuela: 26–29 Jul 1928; 17–22 Jul 1957
Parmenter (1976)	Satellite/synoptic case study	Cross equatorial cold front passage, 14–21 Jul 1995
Hamilton and Tarifa (1978)	Case study using surface, upper air, and satellite imagery	Frost in tropical Brazil, 5–11 Jul 1972
Fortune and Kousky (1983)	Synoptic case studies using surface, upper air, and satellite observations	Two severe freezes in Brazil: 26–31 May 1979; 14–21 Jul 1981
Marengo et al. (1997a)	Synoptic case study using NCEP–NCAR reanalyses	Strong event of 23–27 Jun 1994
Marengo et al. (197b)	Climatology and case studies	Climate impact of cold surges over Amazonia 1983–96
Garreaud and Wallace (1998)	Composite study of warm season cool surges	Uses NCEP–NCAR reanalysis data and OLR data for 1979–95 to get surge structure
Knight and Bosart (1998)	Modeling study (MM5)	Event of 19–21 Jul 1992
Garreaud (1999)	Modeling study (MM5)	Event of 12–15 May 1993
Garreaud (2000)	Mean synoptic structure using NCEP–NCAR reanalyses for 1979–95	Emphasis on physical mechanisms from diagnosis of dynamical and thermodynamical forcing
Nocera et al. (2000)	Climatology–composite	Five-year study of surge types
Bosart et al. (2000)	Modeling study (MM5)	Event of 6–10 Jul 1994
Vera and Vigliarolo (2000)	Composite diagnostic study	Based on ECMWF analyses (1983–88)
Lupo et al. (2001)	Climatology–composite	Categorization by surge type through composites: events of 19–25 Jul 1992 and 13–15 Apr 1993

1950; Quiroz 1984; Konrad and Colucci 1989; Rogers and Rohli 1991; Konrad 1996; Schultz et al. 1997, 1998) and a deep trough over the affected area. In the case of North America, topographical features facilitate the channeling effect of the cold air equatorward (e.g., Colle and Mass 1995; Schultz et al. 1997, 1998). At the surface, these cold surges are associated with the occurrence of strong surface anticyclones and the passage of surface cyclones. Colle and Mass (1995) investigated various possible forcing mechanisms responsible for the propagation of cold surges deep into the North American continent. They determined that the synoptic-scale dynamics associated with these events were advective (temperature and vorticity) and, thus, similar to cold air damming along the east coast of the United States, rather than being associated with Kelvin or topographic Rossby/shelf waves. Schultz et al. (1997) found similar results in their examination of the March 1993 Superstorm cold surge. However, they point out that the surge has some features in common with previously proposed conceptual models such as Kelvin waves, pressure jump lines, bores, and gravity currents. Finally, many of the above studies (e.g., Konrad and Colucci 1989; Rogers and Rohli 1991; Konrad 1996; Schultz et al. 1998) that have examined North American cold surges have attempted to classify these events by their accompanying synoptic and planetary-scale flow characteristics.

Earlier studies of Southern Hemisphere cold surges (e.g., Hamilton and Tarifa 1978; Fortune and Kousky 1983) associate South American cold air surges with strong ridging over South America and the immediate eastern Pacific and troughing over the immediate western Atlantic, resulting in a deep layer of meridional flow over South America that facilitates the channeling of cold air equatorward. These cold air surges have long been associated with a strong surface high pressure region (e.g., Sera and Ratisbona 1945; Myers 1964; Ratisbona 1976). The Andes Cordillera and the eastern Brazilian highlands would also seem to be instrumental in funneling the cold air equatorward as suggested by Hamilton and Tarifa (1978), Fortune and Kousky (1983), and Marengo et al. (1997a), and their effect in aiding the equatorward flow of cold air will be shown in this paper. However, past studies have been limited to the study of surface data (e.g., Sera and Ratisbona 1945), once daily upper air observations (e.g., Hamilton and Tarifa 1978), or satellite imagery analyses (e.g., Parmenter 1976; Fortune and Kousky 1983), and these earlier studies have been hampered by the lack of adequate data coverage over the adjacent ocean basins. Thus, earlier studies, such as Hamilton and Tarifa (1978), have been limited to compiling the sequence of events contributing to cold air surges over the South American continent only. However, the recent availability of global datasets has allowed for more detailed observational and numerical studies of South American cold air surges (e.g., Marengo et al. 1997a; Garreaud and Wallace 1998; Knight and Bosart 1998; Garreaud 1999, 2000; Bosart et al. 2000; Nocera et al. 2000; Vera and Vigliarolo 2000).

A common signature of the South American cold air surge studies listed in Table 1, and one also reflected in the North American cold air surge studies, is the presence of an amplified upper air flow pattern in conjunction with a pronounced surface anticyclone. Garreaud (1999, 2000) has emphasized the importance of both dynamical and orographic forcing on the evolution and structure of South American cold air surges based

upon mesoscale modeling simulations and composite studies. He has proposed a three-stage cold air surge model. In the first stage, cold air sweeps equatorward east of the Andes to near 30°S, primarily in response to large-scale, dynamically induced, quasigeostrophic southerly flow between an advancing anticyclone near the Andes over southern Argentina and a developing cyclone east of Argentina. In the second and third stages, low-level cold air advection drives colder air equatorward in response to a large meridional pressure gradient along the eastern flanks of the Andes that is reinforced by the orographic channeling of cold air to the east of the Andes. Vera and Vigliarolo (2000) provided independent support for the findings of Garreaud (1999, 2000). They also noted the importance of the subtropical jet (STJ) in the stronger cold air surges that could be associated with frost and freezing temperatures deep into subtropical and tropical South America. In these situations a thermally direct secondary circulation in the entrance region of the STJ helped to reinforce the equatorward transport of low-level cold air to the east of the Andes in conjunction with a surface anticyclone.

It is also important to note that cold air surges can occur across northern Argentina and southeastern Brazil in the absence of a major surface anticyclone and highly amplified upper air flow. These situations can arise when a large-scale trough is situated over the eastern Pacific and South America such that the southern and central Andes Cordillera region is embedded in a strong and persistent cyclonic westerly flow that contains predecessor disturbances aloft that can interact with the Andes. This scenario is also associated with a surface cyclone and no discernable major surface anticyclone. Surface cyclogenesis typically occurs west of southern Chile in this environment and is followed by secondary cyclogenesis over coastal southern Argentina. Subsequently, a large mass of maritime polar air, initially situated close to the southern tip of South America, is able to flow equatorward behind the surface cyclone.

This study will examine the dynamic characteristics of both the large- and synoptic-scale aspects of differing types of South American (SA) cold surges. In sections 2 and 3 we classify South American cold surges into three categories based on their occurrence within differing atmospheric flow regimes, the orographic forcing associated with the cold surges, and their association with predominant synoptic-scale features. In section 4 we will present the results from two case studies, one featuring a strong cold surge associated with anticyclogenesis at the surface and aloft, the other featuring a modest cold surge in the wake of explosive cyclogenesis. Both cold surges will also be examined from a potential vorticity (PV) perspective (e.g., Hoskins et al. 1985, hereafter HMR85; Hoskins and Berrisford 1988) to help understand better the important large-scale dynamical control of cold air surges and to facilitate comparison with previous studies. The summary and conclusions follow in section 5.

2. Analyses and diagnostic techniques

a. Analyses

The dataset used in this study was the National Centers for Environmental Prediction (NCEP) and National Center for Atmospheric Research (NCAR) gridded reanalyses [full details can be found in Kalnay et al. (1996)]. These analyses are archived at NCAR and are available from the NCAR mass-store facility. The reanalyses used here are 2.5° by 2.5° latitude–longitude gridded analyses available on 17 mandatory levels from 1000 to 10 hPa at 6-h intervals. These analyses include standard atmospheric variables such as geopotential height, temperature, relative humidity, vertical motion, u and v wind components, a set of various surface fields, and tropopause information. Mandatory pressure level data were interpolated quadratically in ln[p] to 21 levels in 50-hPa increments from 1050 to 50 hPa. Interpolating quadratically in ln[p], as opposed to linearly, produces a robust profile, particularly for the u and v wind components, that more closely resemble raw sounding information (Lupo and Bosart 1999).

b. Diagnostic techniques

The PV framework is adopted as a primary analysis and map display tool. Interested readers should consult Morgan and Nielsen-Gammon (1998, and references therein) for a concise guide on the use and interpretation of PV and dynamic tropopause (DT) maps. The important initial steps taken in developing the concept of PV were performed in Rossby (1940), and independently by Ertel (1942). The history of PV development and the derivations can be found in HMR85 or Pedlosky (1987). This quantity is defined as

$$\mathrm{PV}_\theta = \frac{\boldsymbol{\omega}_a \cdot \boldsymbol{\nabla}\theta}{\rho}, \tag{1}$$

where PV_θ is Ertel's potential vorticity. Here potential temperature (θ) is the vertical coordinate, $\boldsymbol{\omega}_a$ is the three-dimensional absolute vorticity vector, ρ is the density of air, and $\boldsymbol{\nabla}$ is the three-dimensional gradient operator. Note that PV_θ is conserved for inviscid, adiabatic three-dimensional flows (see HMR85; Pedlosky 1987). The conservation property is also the foundation for examining wave development in terms of θ, or some other conserved variable, on a dynamically significant PV surface [e.g., 2.0×10^{-6} K m^2 kg^{-1} s^{-1}, or 2.0 PVU, as in Hoskins and Berrisford (1988) or McIntyre (1988); Nielsen-Gammon and Lefevre (1996); Lackmann et al. (1997)]. Additionally, the global distribution of PV, given a suitable boundary condition and "reference" state, can be used to recover all the relevant dynamical fields such as winds, temperature, and pressure through the "invertibility principle" (HMR85).

In this diagnosis, PV was calculated and examined on isobaric surfaces (e.g., Bosart and Lackmann 1995; Lupo and Bosart 1999). Introducing hydrostatic balance

TABLE 2. Strength criteria for the three types of South American cold surges. The thickness contours identified refer to the nose of the farthest equatorward extent of a 1000–850-dam thickness contour.

Type	Strength	Requirements
Type 1: anticyclone remains west of the Andes Type 2: anticyclone builds east of the Andes	Strong	135 dam reaches 20°S and 138 dam reaches 15°S between 55° and 65°W
	Moderate	135 dam reaches 25°S or 138 dam reaches 15°S between 55° and 65°W
	Weak	135 dam reaches 30°S between 55° and 65°W
Type 3: Anticyclonic cold surge east of the Brazilian coastal mountains	Strong	138 dam reaches 12°S between 40° and 50°W
	Moderate	138 dam reaches 20°S between 40° and 50°W
	Weak	138 dam reaches 27°S between 40° and 50°W

and transforming into isobaric coordinates, the expression in (1) becomes (e.g. HMR85; Bosart and Lackmann 1995)

$$\mathrm{PV} = g\left[\hat{\mathbf{k}} \cdot \left(\frac{\partial \mathbf{V}}{\partial p} \times \nabla\theta\right) + \zeta_a \frac{\partial \theta}{\partial p}\right], \qquad (2)$$

where ζ_a denotes the absolute vorticity. Although PV is not conserved when considering only horizontal motions on isobaric surfaces, researchers (e.g., Bosart and Lackmann 1995; Lupo and Bosart 1999) have shown that this form can be used as an effective diagnostic tool. Also, since pressure and height are the vertical coordinate in the observation network, it is necessary to use numerical interpolation to calculate PV on isentropic surfaces (HMR85), which gives only an approximation to the real PV distribution.

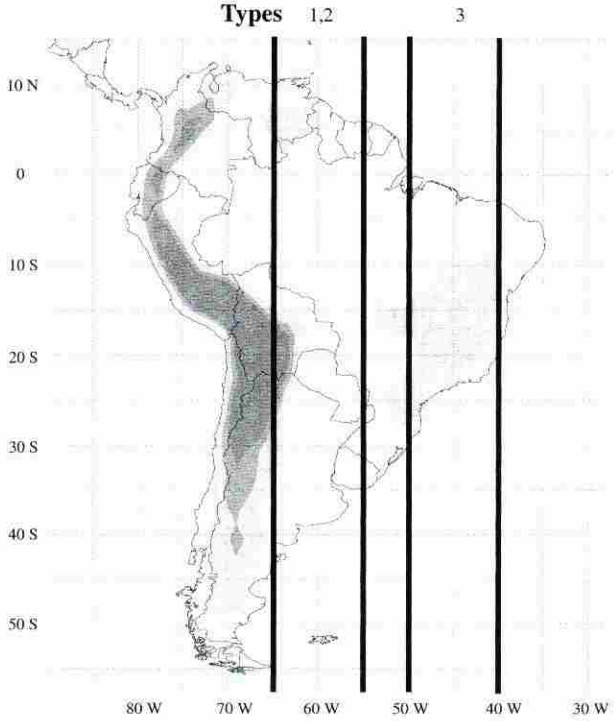

FIG. 1. Longitude regime for each type of cold surge, labeled at the top of the figure. Elevation is shaded: light (>500 m), dark (>1000 m), and darkest (>1500 m).

c. *Climatological classification methodology*

The climatology of South American cold surges was constructed using NCEP–NCAR reanalyses data consisting of 1000-hPa heights and 1000–850-dam thickness contours for a 5-yr period (1992–96) in order to elucidate the different mechanisms responsible for producing cold surges adjacent to higher terrain. Cold surges were classified into three types based on their meridional location and distinctive synoptic-scale features. The meridional criteria for the three cold surge types is given in Table 2 and shown in Fig. 1 and relates the location of the cold surge to the mountain chain that channels the low-level cold air. Type 1 and 2 cold surges occur east of the Andes Mountains while type 3 cold surges occur east of the Brazilian coastal mountains. Type 1 and type 2 cold surges differ in the extent that the Pacific anticyclone remains over the ocean (type 1) or builds eastward across the southern Andes (type 2). As will be demonstrated, type 2 cold surges feature the formation of a strong anticyclone to the east of the Andes over southern Argentina in conjunction with dynamic anticyclogenesis aloft. Type 3 cold surges east of the Brazilian coastal mountains arise either from type 2 cold surges that propagate well equatorward or from lower latitude in situ development. A climatology for each surge type was constructed describing the relative frequency, intensity, and favored season of occurrence.

The three types of cold surges were subdivided into three intensity levels (Table 2). The intensity criteria were subjectively chosen after manual inspection and analysis of surface and upper air weather maps over the 5-yr period defined above. The 1000–850-hPa thickness, a measure of the mean temperature of the lowest layer (~925-hPa) of the atmosphere, was used to help define the intensity of a cold surge. The subjective cold surge identification methodology adopted here necessarily differs from that used in studies of North American cold surges (e.g., Mecikalski and Tilley 1992; Reding 1992; Colle and Mass 1995; Schultz et al. 1997, 1998) because of data limitations. For example, the absence of frequently available surface observations precludes picking one point and reliably assessing cold surge occurrence on the basis of a wind shift, pressure rise, and temperature drop (most South American surface observations are available only every 3 or 6 h and

overnight observations are not always available). Likewise, the limited South American radiosonde data, available only once per day at 1200 UTC at most stations, further complicates using raw upper air observations to define cold surge occurrences.

To partially circumvent these problems we decided to use a consistent set of surrogate mean temperature (~925 hPa) analyses based on the 1000–850-hPa thickness as obtained from the NCEP–NCAR reanalyses. Cold surge intensity was subjectively defined on the basis of the farthest equatorward extension of the 135- or 138-dam 1000–850-hPa thickness contours as gleaned from manual inspection of the NCEP–NCAR reanalysis maps for the 1992–96 period. A measure of the success of our subjective procedure in isolating cold surges can be gleaned from the significance test of the 1000–850-hPa thickness anomalies described in section 3. Note also that any thickness-dependent cold surge definition can result in a seasonal bias since more cold surges will occur during the winter months than during the summer months. However, this study does result in a classification scheme that determines a likelihood of surge occurrence during a part of the cold season.

Composites of each type of cold surge life cycle were calculated in order to understand the differences between each type and to identify their synoptic-scale signatures. The life cycle of each cold surge was examined in a 4-day window centered on the time of the greatest equatorward extent of the 1000–850-hPa 135- or 138-dam thickness contour (defined as $t - 0$ days). The end points are defined as times $t - 2$ (2 days before $t - 0$) and $t + 2$ (2 days after $t - 0$), respectively. It should be noted that the time of each composited grid was kept consistent; that is, 0000 (1200) UTC grids were only composited with 0000 (1200) UTC grids. The compositing times were kept consistent due to spurious (high) height anomalies generated by extrapolating cool temperatures during the 1200 UTC time period to obtain heights below the surface. Thus, day $t - 0$ was defined as the greatest equatorward extent of a cold surge at 0000 UTC. For each type of cold surge, 1000-hPa heights, 1000–850-hPa thicknesses, 500- and 200-hPa heights, and 500- and 200-hPa vorticity advection were composited. Climatological mean fields of height, thickness, and vorticity advection were computed for each surge type by weighting the monthly means in the NCEP–NCAR reanalyses by the number of cold surges occurring in that month. Statistical analysis was then performed using these weighted climatological mean grids. The composited grids were tested for significance using a two-sided t test (e.g., Gujarati 1992). The local statistical significance of relevant synoptic-scale features for each type of surge was tested at the 95% and 99% levels.

In addition to the three types of orographically channeled cold surges described above, we also examined cases of cool changes where no direct orographic signature was evident (e.g., cool air outbreaks to the rear of offshore cyclones). These additional surges occurred when cold air moved equatorward between the Andes and the Brazilian coastal mountains with no significant evidence for cold air damming or orographic channeling of cold air. During the 1992–96 period there were 27 (49) nonorographic cold air surges predominantly associated with equatorward flow on the western (eastern) flank of a cyclone (anticyclone). Although composite results from these types of cold surges will not be presented here, they can provide an important source of dynamically forced cooling not associated with direct influences by the Andes or Brazilian coastal mountains. To reinforce this point, we will show results from the cold surge of 12–14 April 1993 that occurred in the wake of explosive cyclogenesis to the east of Argentina. These explosive cyclogenesis events are comparatively rare, with only four events noted during the 1992–96 period.

3. Composite and climatological characteristics of South American cold surges

a. Synoptic-scale features

Three distinct South American cold surge flow regimes have been identified. We will now proceed to briefly describe each cold surge type and frequency of occurrence, and the characteristic flow regime associated with each surge type.

1) TYPE 1 COLD SURGE

Type 1 cold surges feature a weak secondary anticyclone that builds eastward across Chile into southern Argentina. A composite of the 30 type 1 cases found between 1992 and 1996 appears in Fig. 2. At $t - 2$, an anticyclone lies over the southeast Pacific Ocean west of Chile (Fig. 2a). A pool of anomalously cold air (significant at the 99% level) as measured by the 1000–850-hPa thickness is found over southern South America. This cold pool of air extends equatorward along the west coast of South America to southern Peru and is represented by an equatorward bulge in the 1000–850-hPa thickness contours over the eastern Pacific Ocean. Anomalously warm low-level air (also significant at the 99% level) is confined equatorward of 30°S to the east of the Andes. The 500-hPa anticyclonic vorticity center (AVC) lies poleward of the 1000-hPa anticyclone (Fig. 2b). Anticyclonic vorticity advection at 500 hPa is estimated to occur from the surface anticyclone center to the Chilean coast (Fig. 2b). This anticyclonic vorticity advection lies above an estimated area of low-level cold air advection in the 1000–850-hPa thickness field (Fig. 2a). The 1000-hPa height anomaly map shows that the 1000-hPa heights are significantly higher (significant at the 99% level) than the climatological mean values over the eastern Pacific Ocean (Fig. 2c). This positive 1000-hPa height anomaly reflects the local intensification of

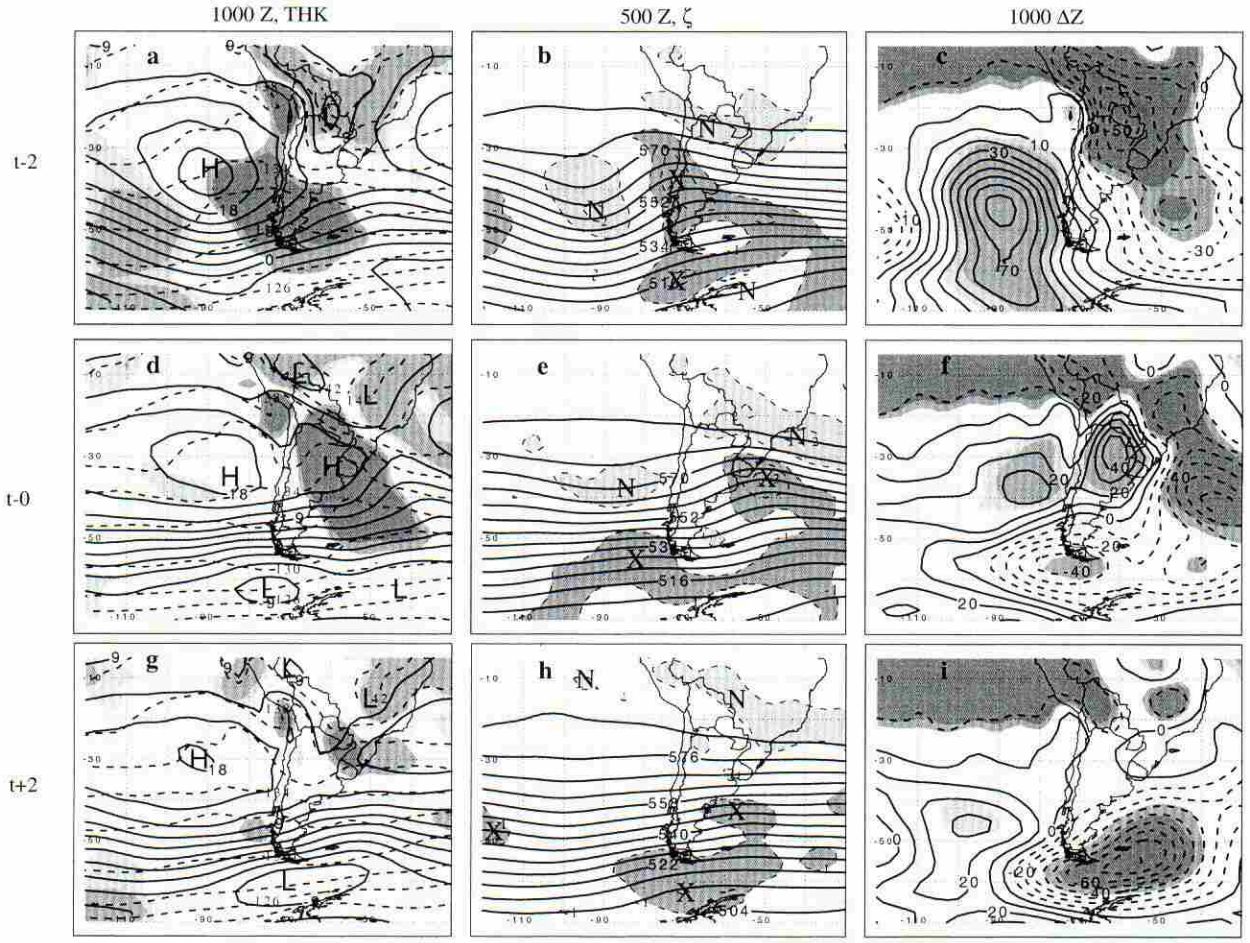

FIG. 2. Type 1 cold surge composite: day $t - 2$ [(a), (b), (c)—top], day $t - 0$ [(d), (e), (f)—middle], day $t + 2$ [(g), (h), (i)—bottom]. (a), (d), and (g): The 1000-hPa height (dam, solid, interval = 3) and 1000–850-hPa thickness (dam, dashed, interval = 2), and statistically significant thickness anomaly, composite-climatological mean; lighter (darker) shading represents positive (negative) anomalies with significance >95%, darker shading within each area represents significance >99%. (b), (e), and (f): The 500-hPa height (dam, solid, interval = 6) and relative vorticity ($\times 10^{-5}$ s^{-1}, dashed, interval = 1), where X (N) represent cyclonic (anticyclonic) centers shaded dark (light). (c), (f), and (i): The 1000-hPa height anomaly, composite-climatological mean (m, solid, interval = 10) and statistical significance; shaded as in (a), (d), and (g).

the quasi-stationary surface anticyclone in the eastern Pacific in response to the passage of a transient short-wave ridge aloft (Fig. 2b). An area of anomalously low 1000-hPa heights is present in the lee trough region to the east of the Andes.

At the time of the greatest equatorward extent of the surge ($t - 0$), the main center of the 1000-hPa anticyclone remains over the eastern Pacific Ocean (Fig. 2d). However, a weaker secondary anticyclone center, represented by an equatorward bulge in the 150-m 1000-hPa height contour, develops east of the Andes in the region of estimated low-level cold air advection and negative 1000–850-hPa thickness anomalies (significant at the 99% level) (Fig. 2d). The equatorward nose of the ridge axis is closely delineated by the 136–138-dam 1000–850-hPa thickness band, which extends equatorward to the east of the Andes to near 25°S (Fig. 2d). At 500 hPa, the primary AVC remains over the eastern Pacific Ocean while a very weak secondary AVC is seen near the southern tip of South America (Fig. 2e). A cyclonic vorticity center (CVC) lies just off the coast of Uruguay over the Atlantic Ocean. Estimated weak anticyclonic vorticity advection (AVA), occurring to the west (upstream) of this CVC, helps to build the 1000-hPa anticyclone eastward across the Andes, leading to the formation of a weak area of high pressure. Although the 1000-hPa positive height anomaly over the eastern Pacific Ocean weakens considerably by $t - 0$, a new 1000-hPa positive height anomaly center forms east of the Andes (significant at the 99% level) in response to general ridging across the mountains (Fig. 2f). The relative absence of 1000-hPa height rises east of the Andes at $t - 0$ reflects the weakening of the transient short-wave ridge aloft (Fig. 2e). Negative 1000-hPa height anomalies and positive 1000–850-hPa thickness anomalies are confined to the northeast of the anticyclone region (Figs. 2d,f).

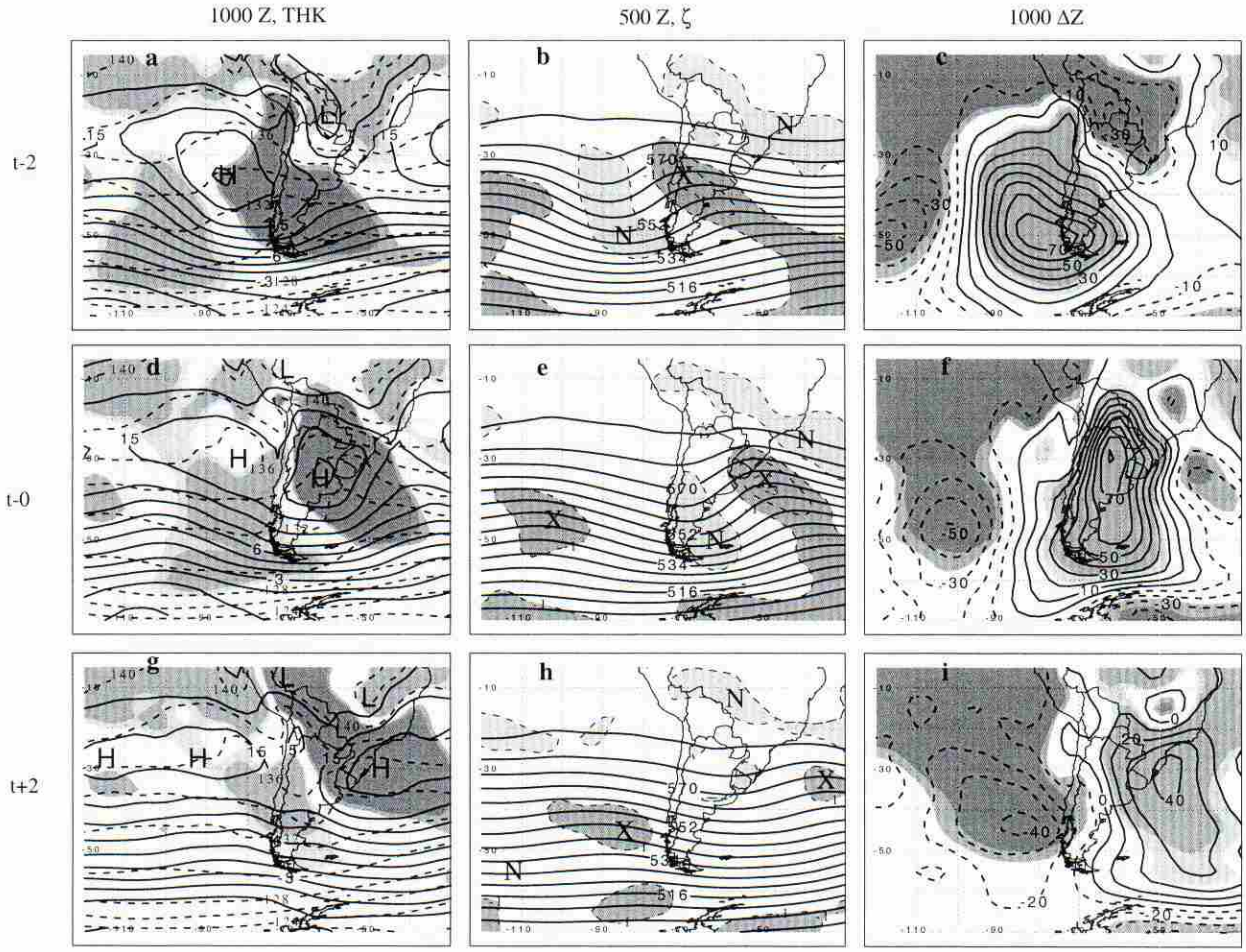

FIG. 3. As in Fig. 2 except for type 2 cold surge composite.

At $t + 2$ the weak area of high pressure located east of the Andes at $t - 0$ all but disappears (Fig. 2g). At 500 hPa the flow has become nearly zonal (Fig. 2h), and there is only a weak CVC located just off the coast of Argentina. Little 500-hPa anticyclonic vorticity advection can be estimated over the disappearing surface anticyclone center east of the Andes. Likewise, the negative 1000–850-hPa thickness anomaly east of the Andes shrinks considerably in comparison to its extent at $t - 0$ (Fig. 2g). The near disappearance of the negative 1000–850-hPa thickness anomaly is also consistent with the dramatic contraction of the area of positive 1000-hPa height anomalies east of the Andes by $t + 2$ (Fig. 2i).

In summary, the type 1 cold surges feature a weak and short-lived surface anticyclone development to the east of the Andes, consistent with the absence of appreciable dynamic anticyclogenesis aloft over southern South America. As a result, type 1 cold surges typically do not produce a widespread cold air outbreak deep into the South American continent since the surface ridge axis remains perpendicular to the Andes instead of parallel to them. This flow configuration will preclude the tapping of much colder air poleward of the ridge axis where the flow is directed away from the Andes.

2) TYPE 2 COLD SURGE

Type 2 cold surges feature a surface anticyclone that develops eastward across the Andes over southern South America. As this anticyclone becomes established east of the Andes the original Pacific anticyclone retreats westward from near the coast of Chile. A total of 62 type 2 cases occurred during 1992–96. At day $t - 2$, an anticyclone is positioned over the Pacific with an indication of ridging across the Andes (Fig. 3a). Both the negative thickness (1000–850 hPa) anomaly associated with the developing cold surge and the positive thickness anomaly associated with the lee trough east of the northern Andes are statistically significant at the 99% level (Fig. 3a). Initially (day $t - 2$) the surge is confined to the eastern Pacific, as represented by the equatorward bulge in the 136-dam thickness contour (Fig. 3a). The 500-hPa AVC lies poleward of the 1000-hPa anticyclone, and a CVC lies over the southern Andes along the Argentina–Chile border (Fig. 3b). AVA

between these two vorticity centers enables the Pacific anticyclone to begin ridging across the southern Andes and supports the formation of a separate positive 1000-hPa height anomaly center (statistically significant at the 99% level) over southern South America and the adjacent eastern Pacific Ocean (Fig. 3c). This positive 1000-hPa height anomaly in conjunction with a statistically significant negative 1000-hPa height anomaly associated with the lee trough also enhances the along-barrier pressure gradient as cold air damming commences east of the Andes (Fig. 3c). Comparison with Fig. 2c also reveals that the 1000-hPa positive height anomaly center is more zonally elongated for the Type 2 composite in response to broader 500-hPa ridging and a stronger (estimated) geostrophic westerly flow at 500 hPa poleward of South America (cf. Figs. 2c and 3c with Figs. 2b and 3b).

By day $t - 0$, a new anticyclone center, enveloped in a pool of anomalously cold 1000–850-hPa thickness (statistically significant at the 99% level), has formed east of the Andes in northeastern Argentina (Fig. 3d). The 136-dam 1000–850-hPa thickness contour now extends equatorward into northern Argentina in conjunction with this cold pool. The 500-hPa AVC has moved eastward to a position to the east of southern Argentina and remains centered poleward of the 1000-hPa anticyclone (Fig. 3e). Meanwhile, the CVC has moved eastward more slowly and now lies just east of Uruguay (Fig. 3e). The resulting shortening of the wavelength between the 500-hPa ridge and the downstream trough and the associated amplification of the flow ensures that in the type 2 composite AVA and the associated forcing for descent overspreads southern South America to the east of the Andes, unlike for the type 1 composite where the AVA forcing is weaker and remains over the Pacific (cf. Figs. 2e and 3e). The propagation of the 500-hPa AVC across the Andes in the type 2 case creates enhanced AVA that eventually supports the development of a surface anticyclone that drives the cold surge. The area of significant positive height anomalies at 1000 hPa has increased in magnitude and shifted both eastward and equatorward (Fig. 3f). It now covers a large area east of the Andes and most of southern South America. This latitudinally extensive positive 1000-hPa height anomaly is the classic signature of cold air damming (note the favorable along-barrier pressure gradient) as the anticyclone ridges equatorward along the eastern slopes of the Andes. Comparison of Figs. 3f and 2f clearly shows that the meridional extent and intensity of the ridging east of the Andes is considerably enhanced in the type 2 composite relative to the type 1 composite. This difference is a manifestation of the aforementioned stronger dynamical forcing aloft in the type 2 composite (Fig. 3e).

By day $t + 2$, the 1000-hPa anticyclone has now propagated off the east coast of South America (Fig. 3g) and is still associated with a significant (99%) negative 1000–850-hPa thickness anomaly. Likewise, the 136-dam 1000–850-hPa thickness contour shows a slight equatorward bulge along the east coast of South America in southeastern Brazil. This bulge is the signature of a type 3 cold surge (to be described more fully below). Although the 500-hPa height pattern has become less amplified, there still is evidence for a weak trough–ridge couplet east of Uruguay and southeastern Brazil (Fig. 3h). Meanwhile, the 1000-hPa positive height anomaly has progressed eastward and weakened (it is still statistically significant at the 99% level). Ridging along the coast of southern Brazil is indicative of the onset of a type 3 surge (Fig. 3i). Clearly, by day $t + 2$ there is a significant difference between the character of the 1000-hPa height anomalies east of the Andes between the type 1 and type 2 composites with weak ridging at 500 hPa just east of southern South America associated with a more robust surface anticyclone for the type 2 surge composite (Fig. 3h).

A summary of the type 2 cold surge reveals that an anticyclone, supported by AVA between a migratory upper-level ridge–trough couplet, moves eastward from the Pacific and reforms east of the Andes Mountains. Once the anticyclone reforms east of the Andes the surface ridge axis becomes oriented parallel to the mountains with a pronounced nose of higher 1000-hPa heights extending well equatorward. A type 2 event will produce the greatest equatorward cold surge as the anticyclone is able to tap cold air from more poleward latitudes and transport it equatorward under the influence of mountain-parallel southerly winds. This type of cold surge is the most widespread and destructive. Most of the published earlier studies summarized in Table 1 examine type 2 cold surges. Type 1 and type 2 cases differ in that the migratory upper-level ridge–trough couplet provides for strong AVA east of the Andes in type 2 cases whereas the only upper-level forcing for type 1 cases is AVA upstream of a migratory trough.

3) TYPE 3 COLD SURGE

A type 3 cold surge features an anticyclone near southeastern Brazil. A total of 164 type 3 cases were found during 1992–96, and the composite results are presented in Fig. 4. Although the magnitudes of the height anomalies are smaller because of the less robust nature of these events, areas of statistically significant anomalies are still present due to the large number of cases in the composite. At day $t - 2$, an anticyclone located over Uruguay with a ridge axis directed toward extreme southern Brazil is represented by a closed 150-m 1000-hPa height contour embedded in a statistically significant (99%) negative 1000–850-hPa thickness anomaly (Fig. 4a). At 500 hPa, a weak ridge lies over central South America and weak AVA downstream of this ridge supports the 1000-hPa anticyclone (Figs. 4b,c). The positive 1000-hPa height anomaly bulges northeastward along the Brazilian coast, a typical signature of the type 3 cold surge (Fig. 4c).

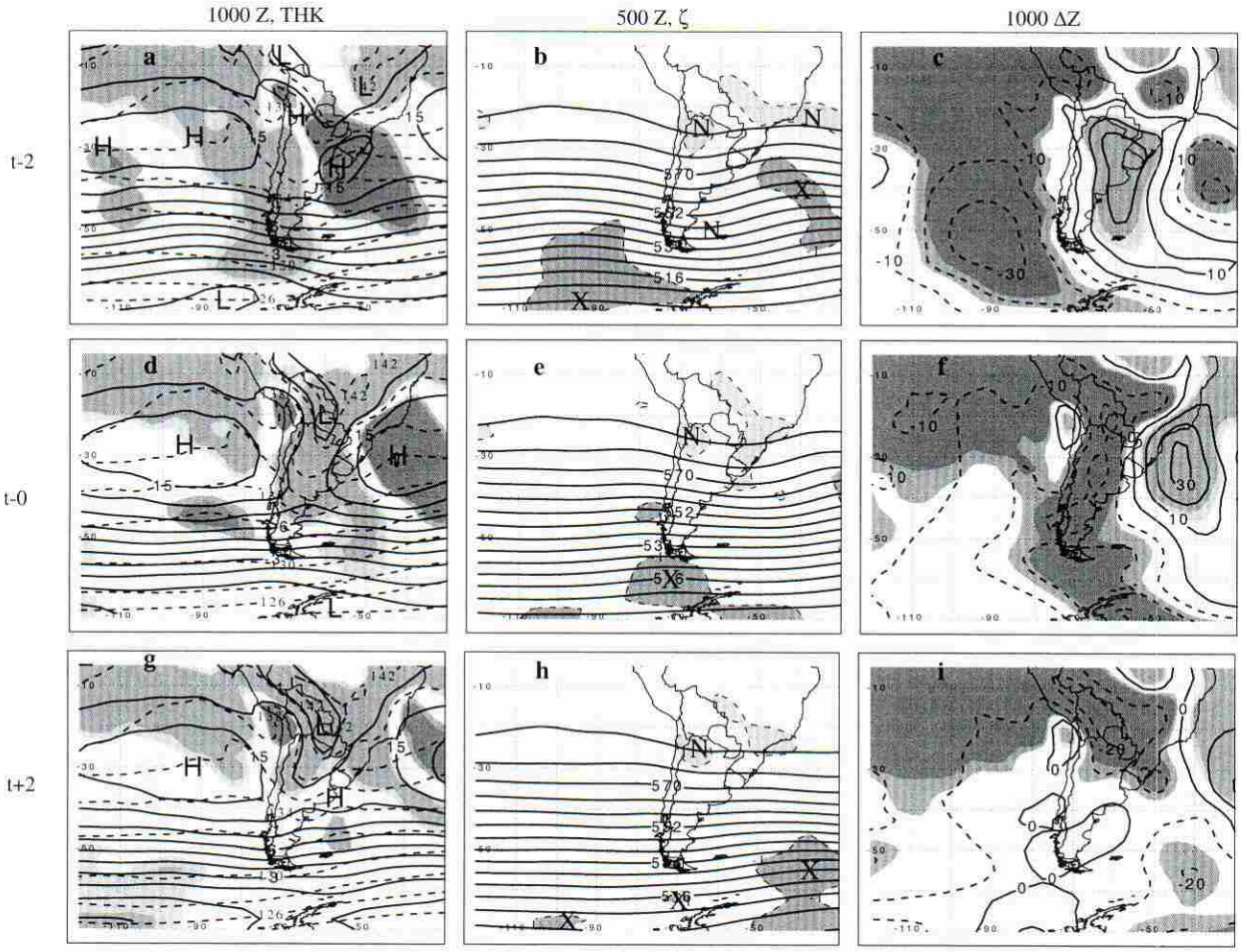

FIG. 4. As in Fig. 2 except for type 3 cold surge composite.

By day $t - 0$, the anticyclone progresses eastward and appears to merge with the Atlantic subtropical anticyclone (Fig. 4d). Cold air damming along the Brazilian coastal mountains is helping to push the 138-dam thickness contour equatorward in a region of statistically significant (99%) negative 1000–850-hPa thickness and positive 1000-hPa height anomalies (Figs. 4d,f). Similarly, a statistically significant lee trough and associated axis of anomalously warm air is apparent east of the Andes (Figs. 4d,f). At 500 hPa, the ridge has moved eastward and is now centered over southeastern Brazil and Uruguay (Fig. 4e). The positive 1000-hPa height anomaly associated with ridging up the coast of Brazil is supported by weak AVA downstream of the ridge at 500 hPa (Figs. 4e,f). Some of the smaller-scale structure of the coastal ridging may also be related to differential diabatic heating across the coastline.

The anticyclone has moved well off the east coast of Brazil by day $t + 2$ (Fig. 4g) while at 500 hPa the flow has become nearly zonal (Fig. 4h). At 1000 hPa the positive height anomaly center seen along the Brazilian coast at day $t - 0$ has disappeared and has been replaced by a northwest–southeast-oriented statistically significant (99%) negative 1000-hPa height anomaly centered over Bolivia (Figs. 4g,i). This feature marks the lee trough that was apparent at day $t - 0$ and now extends poleward to 30°–35°S (Fig. 4i).

In summary, the type 3 cold surge consists of a slow-moving anticyclone off the east coast of Brazil. This leads to easterly flow equatorward of the anticyclone center against the coastal mountains and a cool surge up the east coast of Brazil. Many type 2 cold surges are followed by, or evolve into, type 3 cases as an anticyclone moves eastward across the Andes and southern South America before turning northeastward. As shown in Table 3, nearly 60% (but only 9% of all cold surge cases) of type 2 cold surges were followed by type 3 events. The greatest (smallest) frequency of type 2 to type 3 transitions occurred in 1994 (1993), with around 83% (42%) of type 2 events becoming type 3 events. It is possible that differences in the stationary large-scale (steering) flow, as indicated by the relative frequency of Southern Hemisphere blocking, between these two cold seasons (1993 vs 1994) could explain this result. Many studies of blocking have shown that large-scale flow regimes with slower propagating long

TABLE 3. Total number of type 2 cold surges that were followed by a type 3 cold surge during the 5-yr period of study (1992–96).

Year	Total type 2	Total type 2 followed by type 3	% type 2 followed by type 3
1992	13	7	53.8
1993	12	5	41.7
1994	12	10	83.3
1995	13	9	69.2
1996	12	6	50.0

waves favor blocking events. Wiedenmann and Lupo (1999) found 3 cold season blocking events in 1993 versus 10 events in 1994.

b. *Frequency of each type*

The frequency of occurrence of South American cold surges is presented in Fig. 5. Each type is divided among strong, moderate, and weak cases based on the criteria presented in section 2c (Table 2 and Fig. 1). The monthly (seasonal) distribution of each cold surge type is presented in Table 4 (Table 5). Table 5 demonstrates that cold surges are most common during the winter and spring months (Jun–Nov) and account for 189 of the 256 total events (74%), while 173 of the 256 total number of cold surge events (68%) occur during the *nominal* cold season (defined here as May–Sep). Although this result could be influenced by our thickness-based cold surge definition, as expected, cold surges were most common during the winter months (106). Interestingly, many more cold surges occurred in the spring season (83), than in the fall season (51). This difference is due to an increased frequency of type 3 events in the spring (62) as compared to the fall (30). This suggests that anticyclones may be more common along the east coast of South America during the spring than they are during the fall.

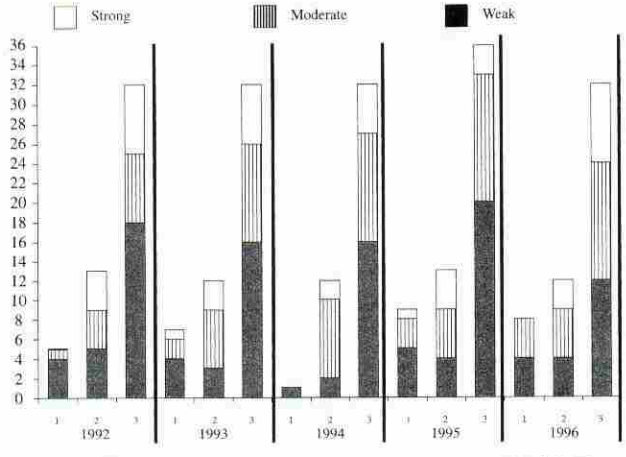

FIG. 5. Frequency of cold surges per year during 1992–96. Type of cold surge is given along the *x* axis with the year given below the types. Number of surges is given along the *y* axis. All surges, except for type 3, were divided into strong, moderate, and weak events as given by the legend at the top.

TABLE 4. Monthly distribution of South American cold surges including totals for anticyclonic and cyclonic surge types.

Month	1 (all)	2 (all)	2 (strong)	3 (all)	3 (strong)	Total
Jan	0	0	0	1	0	1
Feb	2	0	0	1	0	3
Mar	0	1	0	3	0	4
Apr	3	4	0	11	0	18
May	5	8	0	16	2	29
Jun	3	11	5	19	6	33
Jul	6	15	8	19	8	40
Aug	4	9	2	20	10	33
Sep	5	9	1	24	3	38
Oct	1	4	0	21	0	26
Nov	1	1	0	17	0	19
Dec	0	0	0	12	0	12
Total	30	62	16	164	29	256

Type 1 events are most common during the cold season (77% of all type 1), especially in the winter months (43%). The majority of type 1 events are weak to moderate, with an annual average occurrence of six events per year. Generally, five to nine events occurred during any year except for 1994, which featured only one type 1 event (Fig. 5). It is difficult to determine if the paucity of surges during 1994 reflects significant interannual variability (e.g., El Niño–Southern Oscillation related), since the length of the sample is inadequate.

Type 2 surges are more common than type 1 cold surges, with an average annual occurrence of 12–13 events (Fig. 5). These cold surges have a greater tendency to occur during the cold season (84% of the total sample) and winter (56% of the total sample) than type 1 events. Strong type 2 events are confined to the winter months, with all but one event occurring during this season (Table 4).

The average annual occurrence of type 3 cold surges is relatively constant, ranging from 32 to 36 events per year (32.8 events per year) (Fig. 5). This distribution may also reflect the fact that the criterion that defines a type 3 cold surge is weaker than that for type 1 and 2 cold surges. While the largest percentage of type 3 surges occur during the cold season and winter months (60% and 35%, respectively) like type 2 surges, they can occur in significant numbers throughout all seasons and months of the year except January and February.

TABLE 5. Seasonal distribution of South American cold surges including totals for anticyclonic and cyclonic surge types.

Season	1 (all)	2 (all)	2 (strong)	3 (all)	3 (strong)	Total
Summer	2	0	0	14	0	16
Fall	8	13	0	30	2	51
Winter	13	35	15	58	24	106
Spring	7	14	1	62	3	83
Total	30	62	16	164	29	256

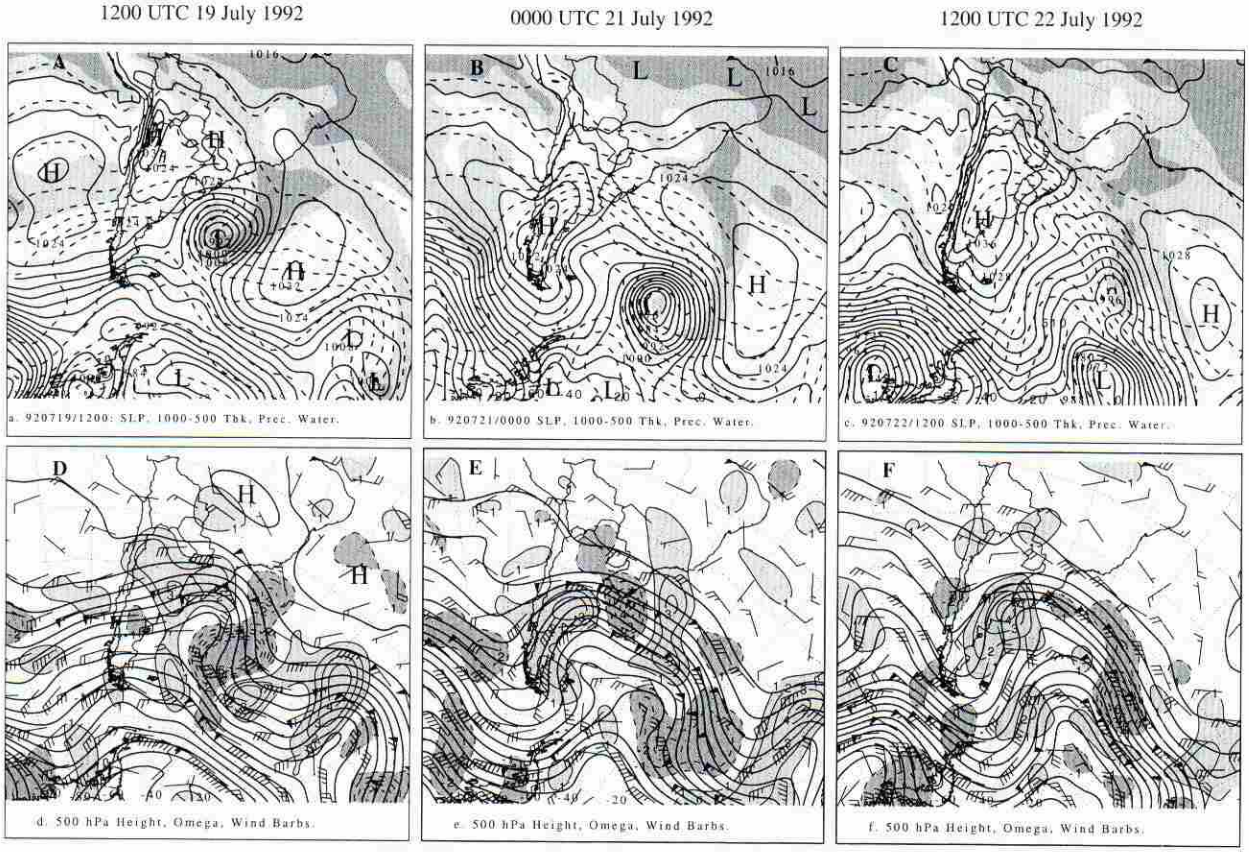

FIG. 6. Jul 1992 Anticyclonic cold surge evolution: 1200 UTC 19 Jul [(a) and (d)—left], 0000 UTC 21 Jul [(b) and (e)—middle], and 1200 UTC 22 Jul [(c) and (f)—right]. (a), (b), and (c): sea level pressure (hPa, solid, interval = 4), 1000–500-hPa thickness (dam, dashed, interval = 6), and precipitable water (mm, light shading >20, dark shading >30). (d), (e), and (f): 500-hPa height (dam, solid, interval = 6), vertical velocity ($\times 10^{-3}$ Pa s^{-1}, interval = 1, dark shading <-1, light shading >1), and wind barbs (1 pennant = 25 m s^{-1}, 1 full barb = 5 m s^{-1}, ½ barb = 2.5 m s^{-1}).

4. Synoptic examples

In this section we show the results from two case studies of cold surges. The first case study is of a common type of cold surge associated with surface and upper-level anticyclogenesis. The second case study illustrates a relatively uncommon type of cold surge that can occur in the wake of strong cyclogenesis.

a. 19–22 July 1992

1) AN ISOBARIC PERSPECTIVE

The 19–22 July 1992 case is illustrative of a strong type 2 cold surge and is similar to many events studied in the past (e.g., Myers 1964; Hamilton and Tarifa 1978; Marengo et al. 1997a,b). It was characterized by a cold air outbreak and accompanying large surface anticyclone. The resulting strong equatorward push of cold air occurred as a two-stage process. Strong cyclogenesis over the southwest Atlantic off the coast of South America drew cold air equatorward to near 25°S in association with an anticyclone (1028+ hPa) centered near Uruguay in the initial (first) stage. Surface and 500-hPa maps for 1200 UTC 19 July shown in Figs. 6a,d are representative of this period. The surface cyclone developed over the previous 24 h (not shown) in association with an upper air trough crossing the Andes and extreme southern Brazil. This cyclone was located along an old low-level baroclinic zone between 25° and 30°S. It then moved southeastward offshore and intensified as warm, moist air was drawn poleward while cold air began to move equatorward in coastal regions from northern Argentina to southern Brazil (Fig. 6a). This scenario is similar to the South American cold air outbreak precursors identified in earlier studies (e.g., Hamilton and Tarifa 1978). In this case, however, the Uruguay anticyclone weakened, moved offshore, and was followed by a very short-lived lee trough and poleward flow east of the Andes Mountains.

Aloft, a well-developed upper air trough embedded in split flow was located over the southwest Atlantic. This trough had crossed the Andes over the previous 48 h and had deepened concurrently with the surface cyclone. The developing surface cyclone was located on the cyclonic shear side of the strongest upper air flow and beneath the poleward-exit region of the upstream

jet maximum (not shown). This location is a favored area for surface cyclogenesis (e.g., Uccellini et al. 1984; Uccellini and Kocin 1987). Subsidence behind the 500-hPa trough over northern Argentina, Uruguay, and southern Brazil is associated with the initial cold push.

By 0000 UTC 21 July the initial weak cold surge had ended as the now intense surface cyclone was well offshore near 50°S and 30°W (Fig. 6b). Weak lee troughing over Paraguay and extreme northern Argentina set the stage for the renewal of an along-barrier pressure gradient in conjunction with a new (primary) cold surge as a second surface anticyclone, initially located west of southern Chile near 45°S, redeveloped east of the Andes and intensified into a 1032+ hPa center over Argentina near 40°S (Fig. 6b). The secondary surge was driven by synoptic-scale ridging aloft near the southern tip of South America (Fig. 6e). This upper-level ridge, evident 36 h earlier at 500 hPa between 90° and 100°W (Fig. 6d), amplified at high latitudes while moving very slowly eastward. The resulting upper-level flow configuration of a high-latitude trough moving eastward poleward of a sharpening trough is a form of anticyclonic synoptic-scale wave breaking (Thorncroft et al. 1993, hereafter THM93). In this case, the wave breaking is associated with the generation of a deep layer of southerly flow aloft over southern Argentina, which supports the equatorward transport of cold air (Fig. 6e). The associated large-scale subsidence between the 500-hPa ridge and the downstream trough supports the surface anticyclogenesis east of the Andes over southern Argentina (Fig. 6e).

By 1200 UTC 22 July the strong type 2 cold surge, now in its mature phase, was marked by an elongated area of high pressure east of the Andes with the pressure nose extending equatorward across Paraguay and Bolivia (Fig. 6c). The intense surface cyclone located near 50°S and 30°W at 0000 21 July (Fig. 6b) has continued moving southeastward toward Antarctica (L1) while a secondary surface trough (L2) has formed along the trailing baroclinic zone beneath strong northwesterly flow aloft (Figs. 6c,f). The 1040-hPa surface anticyclone located upstream of L2 drove the secondary cold air push that reached equatorward to between 25° and 30°S as seen in the 1000–500-hPa thickness (Fig. 6c) and the 850-hPa temperature fields (not shown). Aloft, the upstream ridge located near the southern tip of South America at 0000 UTC 21 July (Fig. 6e) amplified further as it edged very slowly eastward (Fig. 6f). Synoptic-scale subsidence at 500 hPa in the deep southerly flow between this ridge and the still sharp downstream trough continued to support the strong surface anticyclone and strong equatorward cold push (Fig. 6f). Relatively low precipitable water values are also indicative of the deep subsidence in the anticyclone region (Fig. 6c).

The large-scale deep equatorward flow signature found at 1200 UTC 22 July resembles the "traditional" South American cold air outbreak (e.g., Hamilton and Tarifa 1978; Marengo et al. 1997a) described earlier and also bears some similarity to North American cold air outbreaks east of the Rockies (e.g., Keshishian et al. 1994; Colle and Mass 1995; Konrad 1996; Schultz et al. 1997, 1998). The deep and persistent southerly flow is essential if cold air is to reach tropical latitudes of South America. With a strong surface anticyclone in place east of the Andes and deep southerly flow aloft, the stage is also set for cold air damming to play an important role in funneling cold air equatorward through Bolivia and western Brazil (not shown). Note also the nose of higher sea level pressure bulging northeastward along coastal southern Brazil at 1200 UTC 22 July (Fig. 6c). This pressure bulge is the onset signature of cold air damming east of the coastal mountains of southern Brazil and is the initial manifestation of the transition of a type 2 cold surge into a type 3 cold surge that occurs subsequent to 1200 UTC 22 July (not shown).

2) A PV perspective

We next offer a PV perspective on the type 2 cold surge of 19–22 July 1992. The 300-hPa PV [computed from Eq. (2)] and PV advection fields for 1200 UTC 19 July appear in Fig. 7a. A pronounced 300-hPa PV advection couplet associated with the prominent negative PV center east of Uruguay defines the sharp upper-level trough driving the offshore cyclogenesis (cf. Figs. 6a and 7a). Strong positive PV advection behind the prominent negative PV center at 300 hPa can be associated with cold advection at 850 hPa (not shown), sinking motion at 500 hPa (Fig. 6d), and mean sea level pressure rises behind the intensifying offshore cyclone (Fig. 6a). Strong negative PV advection ahead of the prominent negative PV center at 300 hPa can be associated with warm advection at 850 hPa (not shown), ascending motion at 500 hPa (Fig. 6d), and mean sea level pressure falls in conjunction with the offshore cyclogenesis (Fig. 6a).

A second, but weaker, area of positive PV advection at 300 hPa lies over central Argentina immediately upstream of the aforementioned PV couplet (Fig. 7a). However, this second area of weaker positive PV advection ahead of a weak short-wave ridge at 500 hPa was unable to support significant surface anticyclone development in the absence of large-scale ridging aloft and cold advection at low levels (Figs. 6d and 7a). Sea level pressure rises (not shown) behind the cyclone and beneath the region of strong positive PV advection at 300 hPa east of Uruguay and southern Brazil can also be associated with the advection of higher (lower) DT potential temperature (θ_t) [pressure (p_t)], while the reverse is true in the cyclogenesis region near 40°S and 45°W (Figs. 7b,d). Additionally, the most unstable air (Fig. 7c) as indicated by the coupling index (CI; Bosart and Lackmann 1995) is associated with the surface cyclone. The CI is simply the difference between θ_t and the 850-hPa equivalent potential temperature, (θ_e).

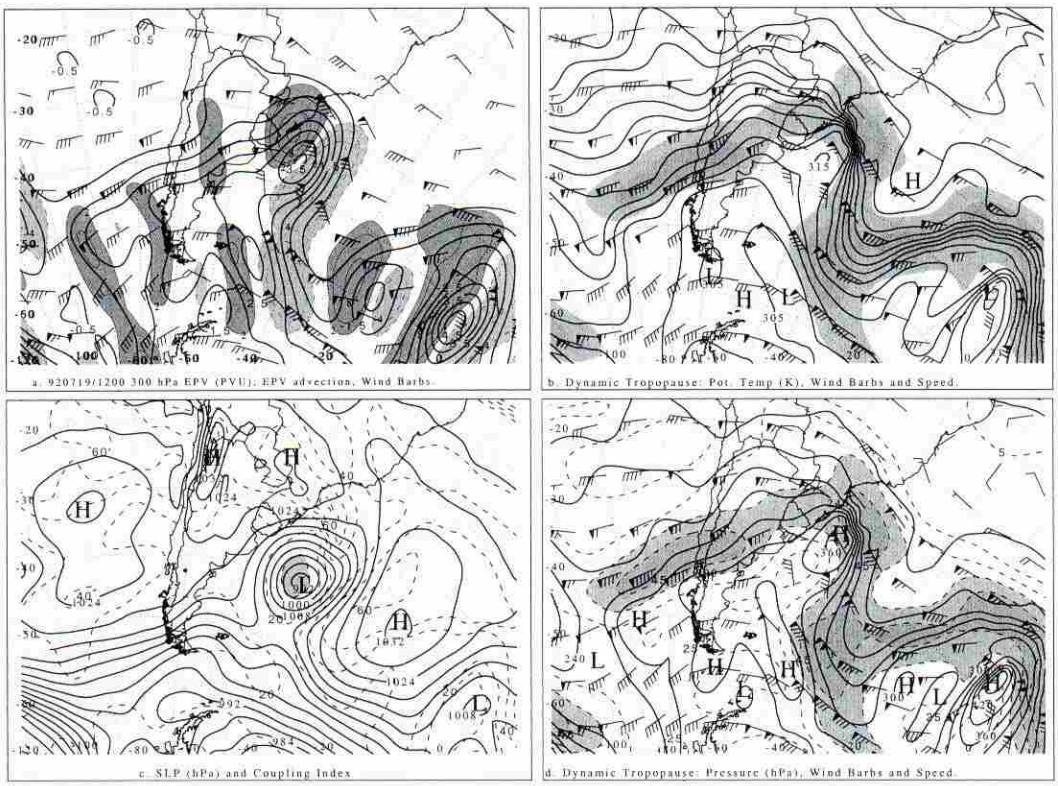

FIG. 7. For 1200 UTC 19 Jul 1992, (a) 300-hPa potential vorticity (PVU, 1 PVU = 10^{-6} m2 K kg^{-1} s^{-1}, solid, interval = 0.5), potential vorticity advection ($\times 10^{-11}$ PVU s^{-1}, light shading <-2, dark shading >2), and 300-hPa wind barbs; (b) dynamic tropopause (2 PVU surface) potential temperature (K, solid, interval = 5), wind speed (m s^{-1}, light shading >35, dark shading >45), and wind barbs; (c) sea level pressure (hPa, solid, interval = 4), and coupling index (K, dashed, interval = 10, shading <10); and (d) dynamic tropopause pressure (hPa, solid, interval = 30), wind speed and wind barbs as in (c).

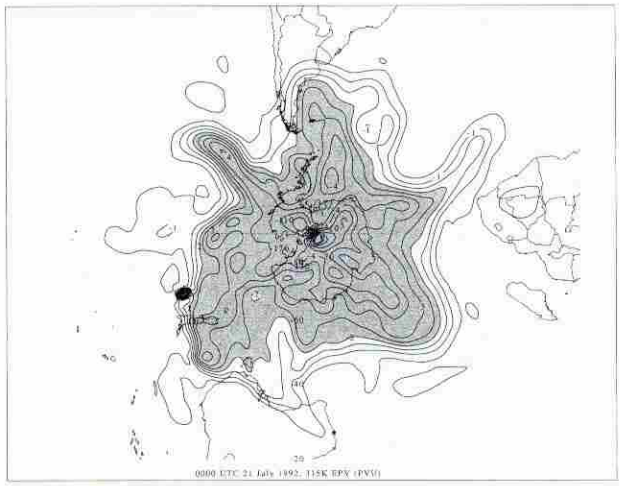

FIG. 8. For 0000 UTC 21 Jul 1992, Ertel potential vorticity (PVU, interval = 0.5, shaded <-2, zero contour omitted) on the 315-K potential temperature surface.

Trough (ridge) regions on the DT are associated with relatively low (high) values of the CI.

Hartmann (1995) showed that the predominance of anticyclonic wave breaking (high-latitude ridge folding over a low-latitude trough; THM93) can be associated with high-amplitude middle-latitude flow regimes in the Southern Hemisphere. An analysis of the development and maintenance of a North American block from a PV perspective by Lupo and Bosart (1999) also supported these associations. By examining the planetary-scale flow for this outbreak in the context of the studies mentioned above, we can gain a qualitative perspective about the role of large-scale forcing in this cold air outbreak. By 1200 UTC 22 July, the 500-hPa flow over South America was highly amplified and a quasi-stationary ridge–trough couplet was located over the South American continent (Fig. 6f). Examination of the 315-K Ertel PV distribution at the intermediate time of 0000 UTC 21 July (Fig. 8), also representative of conditions over the entire midlatitude Southern Hemisphere during the surge period, shows that many of the low (negative) PV extrusions, especially the PV extrusion directly upstream of the amplifying ridge over the central southern Pacific, could also be considered "anticyclonically

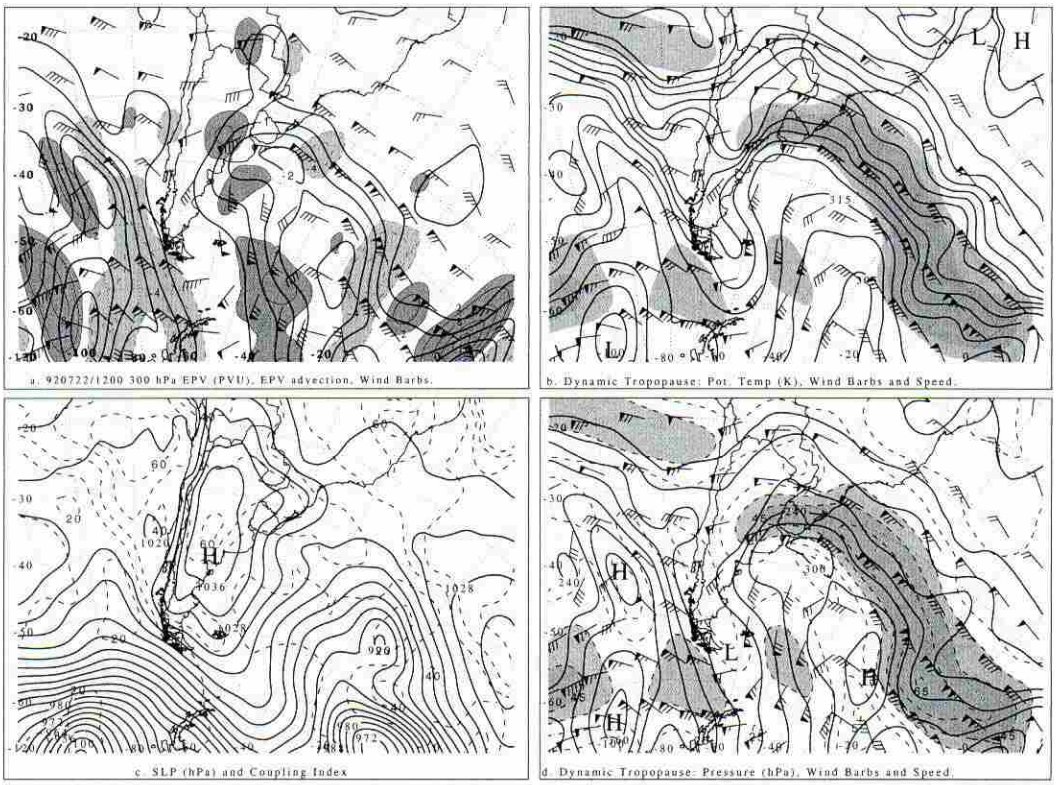

FIG. 9. As in Fig. 7 except for 1200 UTC 22 Jul 1992.

breaking." Figure 8 is similar in appearance to corresponding analyses shown in Hartmann (1995, his Figs. 11 and 13). The hemispheric 500-hPa height analyses (not shown) for this case also shows that the flow in the Southern Hemisphere was dominated by high-amplitude, quasi-stationary, midlatitude waves.

Examination of the PV maps for 1200 UTC 22 July shows that regions of negative PV were located over the Atlantic and Pacific off the each coast of South America (Fig. 9). The PV advection over South America was weak at this time with the strongest positive advection (anticyclonic tendency) located over central Argentina (Fig. 9a). Although the advection of θ_t and p_t (Figs. 9b,d) on the DT were also weak, the advection of higher (lower) θ_t (p_t) over southern Argentina was consistent with ridging aloft and surface anticyclone development. Relatively high CI values located over the poleward portion of the South American continent were indicative of a broad, stable airmass (Fig. 9c). There was also a corridor of high CI values located along the Andes equatorward of 20°S over the Bolivia region. This corridor of high CI values provides additional evidence that cold air was channeled deep into tropical Brazil with the aid of local topographical features during this surge as indicated by the Bella Vista, Bolivia (13°S, 64°W), surface observations (not shown.)

It should also be noted that the local (synoptic scale) environment was made more favorable for the occurrence of a cold surge by the behavior of the larger-scale planetary waves. The planetary-scale flow regime was quasi-stationary and highly amplified, resulting in a deep layer of equatorward flow over South America for a long period of time with respect to the synoptic scale. In addition, as implied by Fig. 8, events occurring far upstream (over the central Pacific) were just as responsible for amplifying the large-scale ridge over South America as synoptic-scale forcing was for building the surface anticyclone. The amplification of the large-scale flow (Fig. 8) may also be due in part to Rossby wave propagation across the South Pacific as forced by anomalous tropical convection. Although Renwick and Revell (1999), for example, have linked Rossby wave propagation and eventual blocking formation to tropical convective forcing in the southeast Pacific region, linking the cold surge to the tropical convection as discussed by them is beyond the scope of this study. We note that highly amplified middle-latitude flow patterns, even ones associated with extensive tropical heating anomalies, can occur without the presence of a block.

In many respects the 19–22 July 1992 South American cold air outbreak event is similar to that of cold air outbreaks occurring over North America in terms of synoptic-scale forcing. (see, e.g., Mecikalski and Tilley 1992; Colle and Mass 1995, Schultz et al. 1997). However, the quasi-stationary and amplified large-scale flow regime is what leads to the type 2 cold surge becoming

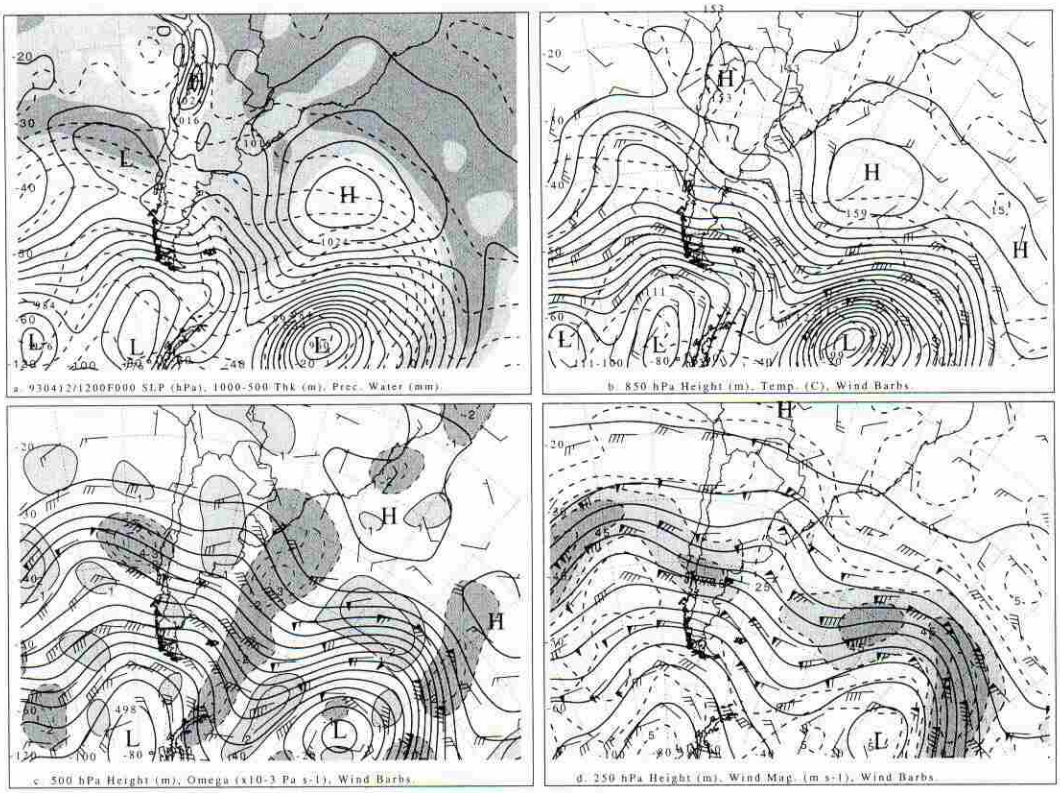

FIG. 10. For 1200 UTC 12 Apr 1993, (a) sea level pressure (hPa, solid, interval = 4), 1000–500-hPa thickness (dam, dashed, interval = 6), and precipitable water (mm, light shading >20, dark shading >30); (b) 850-hPa height (dam, solid, interval = 3), temperature (°C, dashed, interval = 5), and wind barbs; (c) 500-hPa height (dam, solid, interval = 6), vertical velocity ($\times 10^{-3}$ hPa s^{-1}, interval = 1, dark shading <-1, light shading >1), and wind barbs; (d) 250-hPa height (dam, solid, interval = 12), wind speed (m s^{-1}, interval = 10, light shading >35, dark shading >45), and wind barbs as in Fig. 6.

a type 3 cold surge east of the Brazilian coastal mountains after 1200 UTC 22 July (roughly 1800 UTC 23 Jul to 1800 UTC 25 Jul—not shown). As shown above, type 3 cold surges are generally preceded by type 2 cold surges. The transition of the large-scale flow to a more quasi-stationary meridional flow regime as described above contributes to the type 2 surge by creating a deep layer of equatorward flow over South America, and then to the type 3 cold surge by "stalling" the departure of the surface anticyclone from the South American continent. Because the surface anticyclone remains quasi-stationary just downstream of the highly amplified ridge aloft, an extensive meridional airmass movement can result. The outcome of the meridional exchange of air masses is that remnant cool air behind the surge, reinforced by cold air damming east of the Andes, can approach, and sometimes cross, the equator over western Amazonia and, reinforced by cold air damming east of the Brazilian coastal mountains, can also extend down the coast of Brazil toward the equator. Both stages of the 19–22 July 1992 cold surge are manifest as synoptic-scale events that occur within a highly amplified large-scale meridional flow environment, the origin of which may be due in part to events occurring farther upstream over the Pacific Ocean.

b. 12–14 April 1993

1) AN ISOBARIC PERSPECTIVE

We now show an example of a cold surge case that occurred in conjunction with explosive cyclogenesis east of South America (12–14 Apr 1993), but without significant anticyclogenesis at the surface and aloft. Events of this type are comparatively rare with only four cases recorded for the 1992–96 period. It is useful to an examine an "outlier" event such as occurred on 12–14 April 1993 to better compare and contrast the nature of South American cold surges. At 1200 UTC 12 April a weak surface cyclone was approaching Chile near 40°S (Fig. 10a) in association with an upper-level trough embedded in fast westerlies and a low-level baroclinic zone oriented east–west across South America (Figs. 10b,c,d). The surface cyclone was located under the cyclonic shear side and in the poleward-exit region of the 250-hPa jet maximum at this time (Fig. 10d). A tongue of high precipitable water values extends well

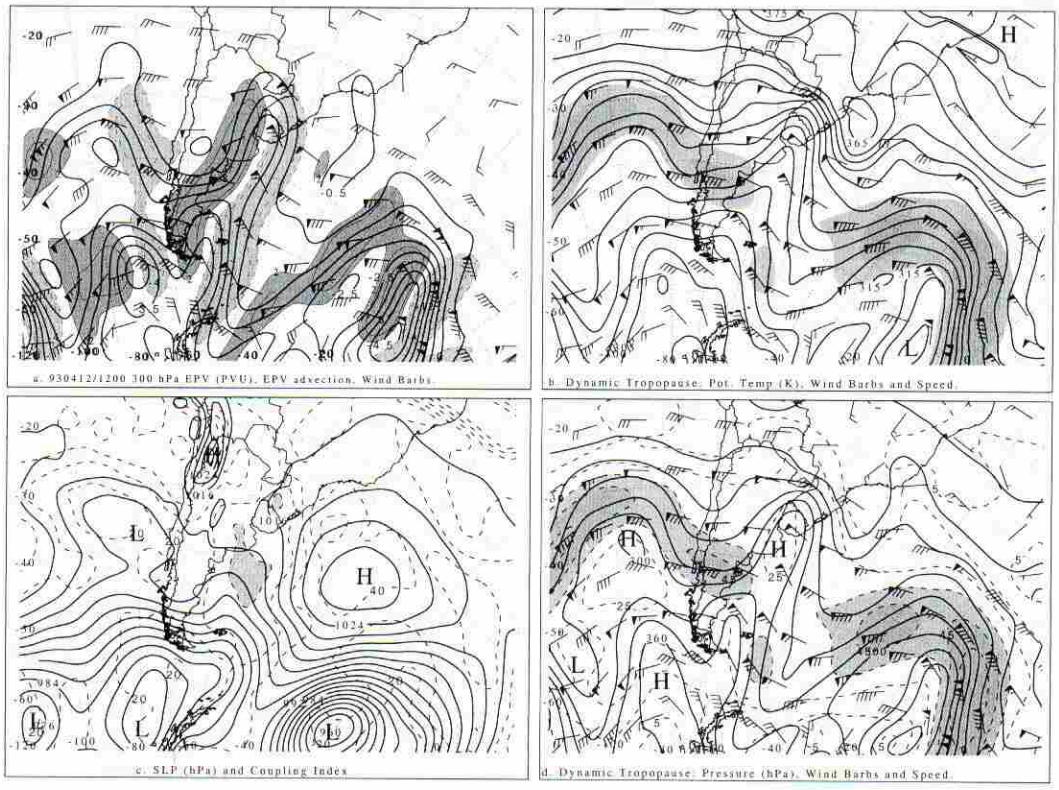

FIG. 11. As in Fig. 10 except for 1200 UTC 14 Apr 1993.

poleward near the east coast of South America in an area of developing low-level northerly flow (Figs. 7a,b). This moist northerly flow can be associated with a meridionally elongated area of ascent at 500 hPa ahead of a weak trough aloft near the east coast of South America (Figs. 10c,d).

The surface cyclone of interest develops east of the Andes and deepens rapidly after moving off the coast of Argentina near 45°S following 0600 UTC 14 April. At 1200 UTC 14 April the strong cyclone, now situated east of Argentina, is embedded in a prominent thermal ridge containing relatively high values of precipitable water (Figs. 11a,b). Although the NCEP–NCAR reanalysis indicated that the cyclone central pressure was 983 hPa at 1200 UTC 14 April, ship observations (not shown) show that this cyclone was much stronger. A ship located near 45°S and 56°W reported a central pressure of 971.1 hPa, a sustained east-northeast wind of 20 m s^{-1}, moderate rain, and a 3-h pressure fall of 19.0 hPa at this time. At 1800 UTC 14 April a second ship located near 44°S and 55°W reported a central pressure of 974.1 hPa, a sustained northwest wind of 30 m s^{-1}, a heavy thunderstorm in progress, and a 3-h pressure rise of 11.5 hPa. The pressure tendency report suggests that the cyclone central pressure must have been below 963 hPa at 1500 UTC 14 April.

Despite this extraordinary explosive cyclogenesis, the cold surge in the wake of the cyclone did not penetrate as deeply into South America as in the July 1992 type 2 cold surge. The generally cyclonic flow aloft over South America behind the cyclone precludes the development of a strong surface anticyclone east of the Andes and associated cold push into low latitudes. According to the 1000–500-hPa thickness and the 850-hPa temperature analyses for 1200 UTC 14 April shown in Figs. 11a,b, the cold surge in the wake of the cyclone overspread most of Argentina and penetrated to at least 30°–35°S. Confirmatory evidence is provided by the surface observations for Cordoba, Argentina (32°S, 65°W), which reveal temperature (dewpoint) decreases of 7°–8°C (10°–15°C), and a sea level pressure rise of almost 18 hPa after the arrival of the surge and wind shift to southerly (not shown). Note also the temperature near 30°C that accompanies the pressure minimum just before 0000 UTC 14 July. This warmth, and modest increase in dewpoint, mark northerly flow lee trough conditions prior to the arrival of the cold surge.

The progression of the trough and cold surge also illustrates the large vector wind shifts that occurred at 850 hPa when strong poleward flow in association with lee troughing and very warm 1000–500-hPa thicknesses (best seen at 1200 UTC 13 Apr; not shown) is replaced by an equally strong equatorward flow following the cold surge (cf. Figs. 10a,b and 11a,b). At 1200 UTC 14 April the closed cyclone at 850 hPa located above the surface storm (Fig. 11b) opens up into a sharp, short-

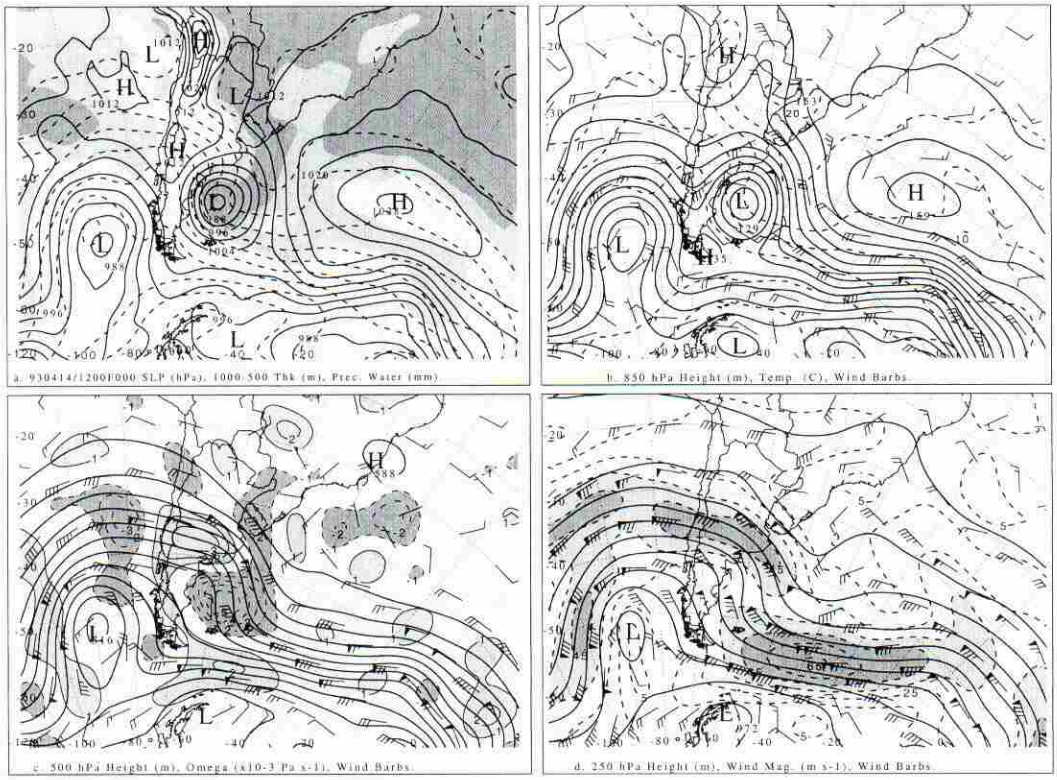

FIG. 12. As in Fig. 7 except for 1200 UTC 12 Apr 1993.

wavelength upper-level trough at 500 and 250 hPa (Figs. 11c,d). Inspection of the 250-hPa map (Fig. 11d) shows that the intense cyclone was situated between two jet maxima (the equatorward-entrance region of the downstream jet and the poleward-exit region of the upstream jet). This jet structure and flow configuration are also known to be favorable for intense cyclogenesis over eastern North America and the adjacent western Atlantic Ocean as was shown by Uccellini and Kocin (1987) and Rogers and Bosart (1991).

The April 1993 case also demonstrates that South American cold surges are not always associated with a large anticyclone and deep equatorward flow aloft. Indeed, the upper-level flow over Argentina remained westerly and northwesterly as intense cyclogenesis proceeded offshore. While the 19–22 July 1992 case exhibits easily recognizable large-scale features, the 12–14 April 1993 case shows that cold surges in South America can occur on smaller scales and can be comparatively shallow events. North American cold surges have also been shown to occur in association with scenarios that differ from more commonly occurring cold air surges as shown by many studies. For example, Hartjenstein and Bleck (1991) show that the severe cold surge of early February 1989, which they called an "orographically ducted" cold surge, was a comparatively shallow event, with a large, cold surface anticyclone sliding equatorward into North America along the eastern slopes of the Rockies beneath west to southwesterly flow at 700 hPa and above. These examples and our own case study results suggest that large-scale dynamical processes, modulated by regional and local physiographic features, play an important role in cold surge life cycles.

2) PV PERSPECTIVE

The PV perspective at 1200 UTC 12 April is shown in Fig. 12. Noteworthy is the large 300-hPa PV (negative) minimum just west of the tip of South America and its equatorward extension to near 25°S (Fig. 12a). Negative PV advection (cyclonic height tendency) at 300 hPa west of Chile is supporting weak surface troughing and cyclone development. Figures 12b,d also show the advection of lower θ_t and higher p_t, respectively, on the DT above the cyclogenesis region west of Chile. These are signatures of cyclone development in the PV framework. Similarly, lower θ_t and higher p_t advection, as well as negative PV advection at 300 hPa, are found in the meridionally oriented trough near the east coast of South America (Figs. 12a,b,d). Also, Fig. 12c shows that a region of relatively low CI values (and thus a region of relatively low static stability) was located in the trough east of Argentina along the moisture axis (Fig. 10a). Thus, conditions were favorable for significant cyclogenesis near the east coast of South America once the prominent trough west of Chile crossed the Andes.

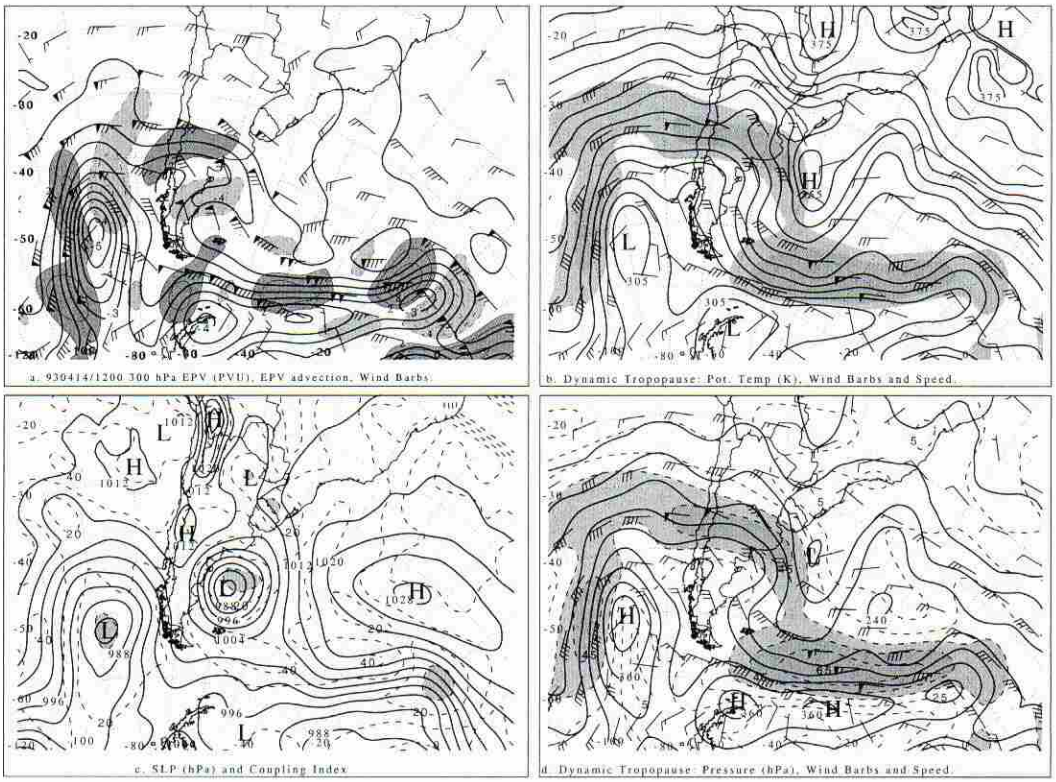

FIG. 13. As in Fig. 7 except for 1200 UTC 14 Apr 1993.

By 1200 UTC 14 April an explosively deepening surface cyclone was situated east of southern Argentina (Fig. 11a). As indicated by the surface observations for Cordoba, Argentina (not shown), cold air was funneling into South America, despite the fact that the flow aloft was northwesterly (Figs. 13a,b,d). As discussed previously, this cold air outbreak was not apparent from examination of the upper-tropospheric maps (Figs. 11c,d) as the relevant features were confined to the lower troposphere. Although no surface ridging was evident, the 850-hPa map (Fig. 11b) demonstrates that cold air advection was occurring over southern Argentina, and Fig. 11a shows that lower 1000–500-hPa thickness values were moving into this same region. An upper-tropospheric vorticity equation analysis (not shown) revealed that vorticity tendencies aloft were weak and even cyclonic over the poleward portion of the cold air outbreak region while larger anticyclonic vorticity tendencies were confined to the equatorward portion of the cold air outbreak region.

A PV analysis (Figs. 13b,d) shows that the positive (negative) PV advection was coincident with the anticyclonic (cyclonic) vorticity tendencies equatorward of the cold air outbreak (Fig. 13a). The PV minimum at this time appeared to be breaking cyclonically in this case as in the sense described by THM93. Also, the advection of lower θ_t and higher p_t (Figs. 13b,d) were favorable to cyclonic development at the surface over the poleward portion of the outbreak region. Thus, it would appear that in the PV diagnostics there is some evidence to suggest that a cold air outbreak is taking place over northern Argentina equatorward of 40°S. Furthermore, as suggested by the PV and vorticity analyses, upper- and lower-tropospheric forcing is still important for ushering cold air equatorward. Hartjenstein and Bleck (1995) and Schultz et al. (1997) found similar results for North American cold air outbreaks.

Examination of the intervening map times (not shown) suggests that the PV extrusions in the South American sector resembled cyclonic wave breaking as described by THM93. Such features would more closely be associated with a low-amplitude flow regime as suggested by the work of Hartmann (1995). The PV features in this regime tended to be more transient in nature. Also, the maps of PV and PV advection in both cases suggested that a major difference between the 19–22 July 1992 and the 12–14 April 1993 cases was that the upper air features were transient in the latter and quasi-stationary in the former. Whereas the planetary scale was important for providing favorable conditions for cold surge propagation in the 19–22 July case, the 12–14 April case was forced by smaller-scale (synoptic and mesoscale) processes. The evolution of the 12–14 April event suggests that it shares characteristics in common with that of the Central American cold surge studied by Schultz et al. (1997), and that topographic forcing may

have played at least a partial role in the cold air outbreak. However, a more detailed study would be needed to validate this hypothesis.

5. Summary and conclusions

A classification scheme and climatology of cold surges for South America was developed by examining synoptic maps of these events over a 5-yr period (1992–96) from which their relative frequency of occurrence was derived. Two cold surge cases studies were performed based on the NCEP–NCAR reanalyses using both a conventional isobaric and a PV framework to help elucidate cold surge dynamics.

The climatological study revealed that South American cold surges could be classified as three types according to their association with surface and upper air features, and just as importantly, topographical forcing. Type 1 cold surges were associated with weak surface anticyclogenesis east of the Andes. The anticyclogenesis occurred in response to the passage of a transient shortwave ridge aloft that first temporarily strengthened the quasi-stationary anticyclone over the eastern Pacific and then weakened as it crossed the Andies [a process also known as anticyclonic "budding"; Sinclair (1996)]. Type 2 cold surges are associated with a more prominent surface anticyclone development east of the Andes in conjunction with dynamical anticyclogenesis aloft. Cold air is channeled equatorward east of the Andes in both type 1 and type 2 surges, but much more prominently in the latter, given the stronger along-barrier pressure gradient between the surface anticyclone and the deeper lee trough and the deep layer of southerly flow that sets up east of the Andes to the east of the ridge axis aloft. Type 3 cold surges occur in conjunction with cold air damming east of the Brazilian coastal mountains. Type 3 cold surges either arise in situ or develop as type 2 surges transition into type 3 surges. The climatology also revealed that cold surges occurred most often during the winter and spring months. Strong cold surges occurred predominantly during the winter months and were primarily type 2 or 3 events.

A case study analysis was made of the strong type 2 cold surge event of 19–22 July 1992. The cold surge occurred in two stages. In the first stage cold air advanced equatorward to 20°–30°S in the wake of surface cyclogenesis that occurred ~15° longitude east of the Argentine coast. Cold air transport farther equatorward was limited by the absence of ridging aloft and associated deep southerly flow. The second stage occurred in conjunction with a significant amplification of the synoptic-scale flow, which, when coupled with a high-amplitude hemispheric flow regime, resulted in the establishment of a deep layer of equatorward-directed flow east of the Andes. A strong surface anticyclone formed east of the Andes beneath an area of strong subsidence at 500 hPa occurring in association with prominent anticyclonic vorticity advection ahead of the ridge aloft. Strong low-level cold air advection ahead of the surface anticyclone in conjunction with cold air damming east of the Andes enabled modified cold air to penetrate deep into tropical Amazonia. The favorable along-barrier pressure gradient for cold air damming was enhanced by lee troughing in the warm air ahead of the surge where the cross-barrier flow was strong. The PV diagnostics showed that the surge could be associated with positive PV advection at 300 hPa, and higher θ_t, advection and lower p_t advection on the dynamic tropopause between the ridge and the downstream trough in the deep southerly flow over southern South America. These features could be associated with the development of the surface anticyclone.

The cold surge of 13–14 April 1993 occurred in conjunction with explosive cyclogenesis east of Argentina. This case differed from the 19–22 July 1992 event in that dynamic anticyclogenesis aloft was absent, no significant surface anticyclone developed east of the Andes, and the flow in mid- and upper levels across the Andes remained northwesterly. The absence of a deep layer of southerly flow and appreciable cold air damming precluded the surface cold surge from reaching beyond 20°–30°S. A PV analysis showed that positive (negative) PV advection was coincident with anticyclonic (cyclonic) vorticity tendencies equatorward of the cold air outbreak. The advection of lower potential temperature and higher pressure on the dynamic tropopause were favorable to cyclone, not anticyclone, development at the surface on the poleward periphery of the cold air outbreak region.

The region encompassed by the cold surge in the 12–14 April 1993 case was smaller in areal extent and did not penetrate as far equatorward as for the 19–22 July 1992 case. The evolution of the large-scale flow also ensured that the cold surge would be more transient so that the threat of frost and cold temperatures over interior South American plains was reduced. Likewise, the surface cyclone underwent explosive development much closer to the coast in the April 1993 case in comparison to the more modest cyclogensesis farther from the coast in the July 1992 case. Given the broad cyclonic environment at low and upper levels in the wake of the April 1993 coastal cyclone (Figs. 10a,c,d and 13a,b,d), conditions were not favorable for surface anticyclone development east of the Andes and resulting cold air damming and equatorward air transport.

Despite the striking differences between both cases, they shared some characteristics in common with each other and with North American cold air surges. Most prominently, upper-tropospheric forcing, as well as 850-hPa cold air advection, were important in generating surface height rises along the leading edge of the cold surge. These signatures were also associated with positive PV advection over northern Argentina in support of weak anticyclogenesis behind a departing cyclone. Finally, in both cases studied here it appears that local

topographical features were important in funneling the cold air equatorward.

Acknowledgments. We would like to thank Dr. Stephen Mudrick and Dr. David M. Schultz for their helpful comments on this manuscript and discussion of results. We thank the anonymous reviewers for their thoughtful and constructive comments and suggestions. This research was supported by the National Science Foundation through Grant ATM-9413012.

REFERENCES

Bosart, L. F., and G. M. Lackmann, 1995: Postlandfall tropical cyclone reintensification in a weakly barotropic environment: A case study of Hurricane David (September 1979). *Mon. Wea. Rev.,* **123,** 3268–3291.

——, J. J. Nocera, and D. J. Knight, 2000: Numerical simulation studies of South American cold air damming: A physical interpretation and assessment. Preprints, *Sixth Conf. on Southern Hemisphere Meteorology and Oceanography,* Santiago, Chile, Amer. Meteor. Soc., 362–363.

Boyle, S., and T.-J. Chen, 1987: Synoptic aspects of the wintertime east Asian monsoon. *Monsoon Meteorology,* C.-P. Chang and T. N. Krisnamurti, Eds., Oxford University Press, 125–160.

Colle, B. A., and C. Mass, 1995: The structure and evolution of cold surges east of the Rocky Mountains. *Mon. Wea. Rev.,* **123,** 2577–2610.

Ertel, H., 1942: Ein neuer hydrodynamischer. *Wirbesatz. Meteor. Z.,* **59,** 277–281.

Fortune, M., and V. E. Kousky, 1983: Two severe freezes in Brazil: Precursors and synoptic evolution. *Mon. Wea. Rev.,* **111,** 181–196.

Garreaud, R. D., 1999: Cold air incursions over subtropical South America: A numerical case study. *Mon. Wea. Rev.,* **127,** 2823–2853.

——, 2000: Cold air incursions over subtropical and tropical South America: Mean structure and dynamics. *Mon. Wea. Rev.,* **128,** 2544–2549.

——, and J. M. Wallace, 1998: Summertime incursions of midlatitude air into tropical and subtropical South America. *Mon. Wea. Rev.,* **126,** 2713–2733.

Gujarati, D., 1992: *Essentials of Econometrics.* McGraw-Hill, 466 pp.

Hamilton, M. G., and J. R. Tarifa, 1978: Synoptic aspects of a polar outbreak leading to frost in tropical Bazil, July 1972. *Mon. Wea. Rev.,* **106,** 1545–1556.

Hartjenstein, G., and R. Bleck, 1991: Factors affecting cold-air outbreaks east of the Rocky Mountains. *Mon. Wea. Rev.,* **119,** 2280–2292.

Hartmann, D. L., 1995: A PV view of zonal flow vacillation. *J. Atmos. Sci.,* **52,** 2561–2572.

Hoskins, B. J., and P. Berrisford, 1988: A potential vorticity perspective of the storm of 15–16 October 1987. *Weather,* **43,** 122–129.

——, M. E. McIntyre, and A. W. Robertson, 1985: On the use and significance of isentropic potential vorticity maps. *Quart. J. Roy. Meteor. Soc.,* **111,** 877–946.

Kalnay, E., and Coauthors, 1996: The NCEP/NCAR 40-Year Reanalysis Project. *Bull. Amer. Meteor. Soc.,* **77,** 437–471.

Keshishian, L. G., L. F. Bosart, and W. E. Bracken, 1994: Inverted troughs and cyclogenesis over interior North America: A limited regional climatology and case studies. *Mon. Wea. Rev.,* **122,** 565–607.

Knight, J. D., and L. F. Bosart, 1998: A modelling study of South American cold air damming and frontogenesis east of the Andes. Preprints, *Eighth Conf. on Mountain Meteorology,* Flagstaff, AZ, Amer. Meteor. Soc., 268–269.

Konrad, C. E., II, 1996: Relationships between the intensity of cold air outbreaks and the evolution of synoptic and planetary-scale features over North America. *Mon. Wea. Rev.,* **124,** 1067–1083.

——, and S. J. Colucci, 1989: An examination of extreme cold air outbreaks over eastern North America. *Mon. Wea. Rev.,* **117,** 2687–2700.

Lackmann, G. M., D. Keyser, and L. F. Bosart, 1997: A characteristic life cycle of upper-tropospheric cyclogenetic precursors during the Experiment on Rapidly Intensifying Cyclones over the Atlantic (ERICA). *Mon. Wea. Rev.,* **125,** 2729–2758.

Lupo, A. R., and L. F. Bosart, 1999: An analysis of a relatively rare case of continental blocking. *Quart. J. Roy. Meteor. Soc.,* **125,** 107–138.

Marengo, J., A. Cornejo, P. Satyamurty, C. Nobre, and W. Sea, 1997a: Cold surges in tropical and extratropical South America: The strong event in June 1994. *Mon. Wea. Rev.,* **125,** 2759–2786.

——, C. Nobre, and A. Culf, 1997b: Climatic impacts of "friagems" in forested and deforested regions in the Amazon Basin. *J. Appl. Meteor.,* **36,** 1553–1566.

McIntyre, M., 1988: The dynamical significance of isentropic distributions of potential vorticity and low-level distributions of potential temperature. *Proc. The Nature and Prediction of Extratropical Weather Systems,* Vol. I, Reading, United Kingdom, European Centre for Medium-Range Weather Forecasts, 237–259.

Mecikalski, J. R., and J. S. Tilley, 1992: Cold surges along the Front Range of the Rocky Mountains: Development of a classification scheme. *Meteor. Atmos. Phys.,* **48,** 249–271.

Morgan, M. C., and J. W. Nielsen-Gammon, 1998: Using tropopause maps to diagnose midlatitude weather systems. *Mon. Wea. Rev.,* **126,** 2555–2579.

Myers, V. A., 1964: A cold front invasion of southern Venezuela. *Mon. Wea. Rev.,* **92,** 513–521.

Nielsen-Gammon, J. W., and R. J. Lefevre, 1996: Piecewise tendency diagnosis of dynamical processes governing the development of an upper-tropospheric trough. *J. Atmos. Sci.,* **53,** 3120–3142.

Nocera, J. J., L. F. Bosart, and D. J. Knight, 2000: A climatology and compositing study of cold surges in South America. Preprints, *Sixth Conf. on Southern Hemisphere Meteorology and Oceanography,* Santiago, Chile, Amer. Meteor. Soc., 378–379.

Parmenter, F., 1976: A Southern Hemisphere cold front passage at the equator. *Bull. Amer. Meteor. Soc.,* **57,** 1435–1440.

Pedlosky, J., 1987: *Geophysical Fluid Dynamics.* 2d ed. Springer-Verlag, 710 pp.

Quiroz, R. S., 1984: The climate of the 1983–84 winter: A season of strong blocking and severe cold in North America. *Mon. Wea. Rev.,* **112,** 1894–1912.

Ratisbona, C. R., 1976: The climate of Brazil. *Climates of Central and South America,* W. Schwerdtfeger and H. E. Landsberg, Eds., *World Survey of Climatology,* Vol. 12, Elsevier, 219–293.

Reding, P. J., 1992: The Central American cold surge: An observational analysis of the deep southward penetration of North American cold fronts. M.S. thesis, Dept of Meteorology, Texas A&M University, College Station, TX, 177 pp.

Renwick, J. A., and M. J. Revell, 1999: Blocking over the South Pacific and Rossby wave propagation. *Mon. Wea. Rev.,* **127,** 2233–2247.

Rex, D. F., 1950: Blocking action in the middle tropospheric westerlies and its effect on regional climate: Part 1. An aerological study of blocking action. *Tellus,* **2,** 196–211.

Rogers, E., and L. F. Bosart, 1991: A diagnostic study of two intense oceanic cyclones. *Mon. Wea. Rev.,* **119,** 1084–1099.

Rogers, J., and R. Rohli, 1991: Florida citrus freezes and polar anticyclones in the Great Plains. *J. Climate,* **4,** 1103–1113.

Rossby, C.-G., 1940: Planetary flow patterns in the atmosphere. *Quart. J. Roy. Meteor. Soc.,* **66,** 68–87.

Schultz, D. M., W. E. Bracken, L. F. Bosart, G. J. Hakim, M. A. Bedrick, M. J. Dickinson, and K. R. Tyle, 1997: The 1993 su-

perstorm cold surge: Frontal structure, gap flow, and tropical impact. *Mon. Wea. Rev.,* **125,** 5–39.
——, W. E. Bracken, and L. F. Bosart, 1998: Planetary and synoptic-scale signatures associated with Central American cold surges. *Mon. Wea. Rev.,* **126,** 5–27.
Sera, A., and L. Ratisbona, 1945: As ondas de frio da Bacia Amazonica. *Bol. Geograf.,* **26,** 172–206.
Sinclair, M. R., 1996: A climatology of anticyclones and blocking in the Southern Hemisphere. *Mon. Wea. Rev.,* **124,** 245–263.
Thorncroft, C. D., B. J. Hoskins, and M. E. McIntyre, 1993: Two paradigms of baroclinic life-cycle behavior. *Quart. J. Roy. Meteor. Soc.,* **119,** 17–55.
Uccellini, L. W., and P. J. Kocin, 1987: The interaction of jet streak circulations during heavy snow events along the east coast of the United States. *Wea. Forecasting,* **2,** 289–308.
——, ——, R. A. Petersen, C. H. Wash, and K. F. Brill, 1984: The Presidents' Day cyclone of 18–19 February 1979: Synoptic overview and analysis of the subtropical jet streak influencing the precyclogenetic period. *Mon. Wea. Rev.,* **112,** 31–55.
Vera, C. S., and P. K. Vigliarolo, 2000: A diagnostic study of cold-air outbreaks over South America. *Mon. Wea. Rev.,* **128,** 3–24.
Wiedenmann, J. M., and A. R. Lupo, 1999: A 15-year global climatology of blocking anticyclones. Preprints, *Eighth Conf. on Climate Variations,* Denver, CO, Amer. Meteor. Soc., 34–37.